

A close-up photograph of a vibrant green tree frog clinging to a smooth, reddish-brown tree branch. The frog is positioned vertically, with its body facing right. Its large, prominent eyes are visible, and its skin has a fine, granular texture. The frog's feet are spread out, gripping the branch. The background is a soft, out-of-focus green, suggesting a natural, forest-like environment.

# Development of a capillary force measurement system for wet adhesion

Camiel H. Jongerius



# Development of a capillary force measurement system for wet adhesion

by

Camiel H. Jongerius

to obtain the degree of Master of Science  
at the Delft University of Technology,  
to be defended publicly on Wednesday November 10, 2021 at 3:00 PM.

Student number: 4389182  
Project duration: February 24, 2020 – November 10, 2021  
Thesis committee: Dr. D. Dodou, TU Delft, supervisor  
Dr. J. Langowski, Wageningen UR, supervisor  
Dr. P. Sharma, Wageningen UR, supervisor  
Dr. B. Bera, TU Delft

An electronic version of this thesis is available at <http://repository.tudelft.nl/>.





## Acknowledgement

I would first like to thank the Experimental Zoology Group (EZO) and the Wageningen University and Research (WUR) for welcoming me and allowing me to take on this project.

I would like to give my special thanks to my supervisors, Dr. Julian Langowski, Dr. Dimitra Dodou and Dr. Preeti Sharma for supporting me and guiding me throughout every step of this thesis.

I would also like to thank Remco Pieters and Henk Schipper for the various help in the laboratories, and with the preparation and acquirement of the components for the system.

I would also like to thank everybody at EZO for being a welcoming group and helping out whenever possible.

Finally, I would like to thank my parents for being supportive and helping whenever they could.

## Abstract

The study of adhesion mechanisms in animals such as the gecko has helped mankind with the understanding and development of novel adhesives. The adhesion mechanism of the tree frog is not fully understood, it is a wet adhesion mechanism which works differently than the dry adhesion mechanisms of animals, such as the gecko, studied previously. The wet adhesion mechanism of the tree frog may be based on the capillary force present in liquids. Researching the adhesion mechanisms of the tree frog could help develop new capillary based adhesives. Although there are several capillary measurement methods and devices used to study the interactions between small volumes of liquids and surfaces, they would require the frog to be immobilized for accurate measurements, which constitutes as harm. This thesis begins the design and development of a system to measure the capillary force created by tree frogs without harming them. The selected concept functions with the use of a pressure sensor connected to the capillary pressure source with capillary channels. This concept allows for a precision of 12 Pa determined by the pressure sensor and a responsiveness of 30 ms determined by fluidic circuit while allowing the frog to roam free around the system input. The components were tested to verify their functionality. A controlled pressure source is used to verify the calibration of the sensor, the time constant and hydraulic capacitance; which are the parameters that determine the accuracy and responsiveness of the system. The sensor was successfully calibrated to measure pressure linearly up to 10 kPa but the time constant and hydraulic capacitance were experimentally measured to be three orders of magnitude larger than the estimated parameters of the components. In order to solve the disparity between the experimental and theoretical values, different tubing and connections were suggested to reduce the hydraulic capacitance and a method verifying the presence of air bubbles was advised. A sessile drop experiment was performed on the pressure sensor in order to support the principle of measurement, the results suggests the principle of measurement is valid but the issues surrounding the fluidic circuit needs to be resolved in order to complete the system.

# Contents

<b>1</b>	<b>Introduction</b>	<b>1</b>
<b>2</b>	<b>Theoretical background information</b>	<b>2</b>
2.1	Theory on capillary interactions . . . . .	2
2.2	Wet adhesion in tree frogs . . . . .	3
<b>3</b>	<b>Concept development</b>	<b>5</b>
3.1	List of requirements . . . . .	5
3.2	Concept Creation . . . . .	6
3.2.1	Meniscus shape . . . . .	6
3.2.2	Area . . . . .	7
3.2.3	Force or pressure . . . . .	7
3.3	Concept Selection . . . . .	9
<b>4</b>	<b>System development for capillary pressure measurement</b>	<b>11</b>
4.1	Measurement principle . . . . .	11
4.2	Component selection . . . . .	12
4.2.1	Hydraulic capacitor . . . . .	12
4.2.2	Cameras . . . . .	13
4.2.3	Substrate . . . . .	13
4.2.4	Tube . . . . .	14
4.2.5	Liquid medium . . . . .	15
4.2.6	Additional components . . . . .	16
4.3	System assembly . . . . .	16
<b>5</b>	<b>System functionality measurements</b>	<b>18</b>
5.1	Calibrating and verifying the working range of the pressure sensor used as a hydraulic capacitor . . . . .	18
5.2	Sensor noise evaluation . . . . .	21
5.3	Evaluating the hydraulic capacitance . . . . .	23
5.4	Additional support for the concept . . . . .	24
<b>6</b>	<b>Conclusion and recommendations</b>	<b>28</b>
<b>A</b>	<b>Calculations to support the component selection</b>	<b>34</b>
<b>B</b>	<b>Additional support to neglect the hydraulic capacitance of the substrate</b>	<b>34</b>
<b>C</b>	<b>Future steps to accomplish</b>	<b>35</b>
<b>D</b>	<b>Verification of the hydraulic capacitance verification method</b>	<b>35</b>
<b>E</b>	<b>Air bubble effect on hydraulic capacitance</b>	<b>36</b>
<b>F</b>	<b>Vibrations additional details</b>	<b>37</b>
<b>G</b>	<b>Proof of concept experiments additional details</b>	<b>38</b>

# 1 Introduction

Mankind has improved the development of adhesives by mimicking the adhesion mechanisms of animals such as the gecko [1–3]. To mimic these animals, the fundamental principles, the conditions and the limitations of their gripping mechanisms have to be studied. Tree frogs differ from other terrestrial animals with gripping mechanisms as they have evolved a form of adhesion through the wetness of their toe pads, the adhesion method is called wet adhesion. The tree frogs wet adhesion is versatile as it can stick to smooth, rough, dry and even wet surfaces found in rainforests. The tree frogs adhesion is adapted to work in a wet environment while maintaining high mobility which can be used to develop new fast wet adhesion mechanisms for commercial use in wet conditions like rainy locations [4].

Many possible underlying mechanisms have been hypothesised to explain the tree frogs' wet adhesion. Currently, the capillary force has been the predominant mechanism according to literature. However, other mechanisms such as the Van der Waals force may be of greater or similar importance as the capillary force [5]. To verify the importance of the capillary force in tree frog adhesion, the capillary force needs to be quantified. Determining the contribution of the capillary force will also suggest if another mechanism is of lower, equal or greater importance in tree frog adhesion. Quantifying the contribution of the capillary force will help select which mechanisms to utilize during the development of potential synthetic wet adhesives.

There are currently several methods used to determine the capillary force in general, which can be classified into three groups: force measurement, liquid shape analysis and pressure measurement. These methods are characterised by different advantages and disadvantages. The force measurement and pressure measurement methods are usually very precise but require a certain control over the subject [6–8]. In force measurement methods, the subject needs to be motionless to reduce the hydro-dynamic force caused by the viscosity of the liquid. This means that the frog would have to be held in place. The liquid shape analysis methods do not require much control over the subject as they ignore forces, like the hydro-dynamic force; but they are usually less precise than the other methods, especially with complex shape like a tree frogs toe pad [9; 10]. There are currently no systems that can measure the capillary force used by frogs in a precise manner, in real time that does not negatively affect the frog; therefore, the aim of this thesis is to develop such a system.

Current knowledge about the functionality of the tree frog adhesion as well as knowledge about the capillary force found in literature will be used to create the initial concepts of the system. This knowledge will also help to validate the final system through analytical calculations. The design of the system will include a setup for a final test, using a liquid meniscus of known parameters applied by a mobile force sensor system to mimic the mucus of the frog. The system will be designed, developed and tested to measure the capillary force of simple adhesive systems.

## 2 Theoretical background information

### 2.1 Theory on capillary interactions

Capillary interactions occur in a multi-phase interface with fluids and solids. The interface is the location at which different phases meet and interact with one another. A bubble in a liquid is a common example of a two-phase interface while a droplet of water on a solid material or a drop of oil on the surface of water are common examples of a three-phase interface. The multi-phase interaction occurring at the toe's of a tree frog is a three-phase interface between the liquid mucus, the gas air and the solid substrate on one side and toe pad on the other.

Starting from a two-phase system, the cohesive force attracts liquid molecules to each other and the adhesive force attracts the liquid molecules to the other fluid. If the cohesive force is significant compared to the adhesion force, the molecules at the surface of a drop will be attracted towards the center of the drop creating the surface separating the liquid from outside, which can be seen in figure 1. The total force over the length of the surface maintaining the shape of the drop is the surface tension, see equation 1. The surface tension varies depending on relative air humidity (%RH), temperature and external pressure [10–12].

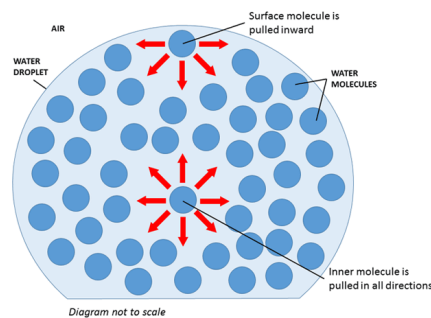


Figure 1: Schematic of the cohesive force at the edge and at the center of a liquid

$$\gamma = \frac{F_S}{L} \quad (1)$$

Where  $F_S$  is referred to as the surface tension force and  $L$  is the unit length the force is acting on. Due to the surface tension being a force which maintains the shape of the liquid, a balancing force is present as pressure. The pressure inside the liquid will be different than the pressure outside. The pressure difference between the two phases at the interface is in balance with the surface tension, which is represented by the Young-Laplace equation:

$$P_c = \gamma * \left( \frac{1}{R_1} + \frac{1}{R_2} \right) \quad (2)$$

Where  $R_1$  and  $R_2$  are the defining radii of curvature of the meniscus. In a perfect sphere i.e. a simplified droplet,  $R_1 = R_2$  [13]. The capillary pressure, also called the Laplace pressure, is the pressure difference between inside the liquid, and outside the liquid. The resulting force, the pressure force, can be determine by multiplying the capillary pressure with the effective area  $A$ , the cross section at the center of the liquid system, see equation 4.

$$P_c = P_{outside} - P_{inside} \quad (3)$$

$$P_c = \frac{F_P}{A} \quad (4)$$

In a three-phase system, the adhesion force is affected by another fluid or solid at the interface. The ratio between the cohesive force and adhesive force is visible from the contact angle  $\theta$ , in which case a larger cohesive force compared to the adhesive force results in a larger contact angle. The surface tension force depends on the contact angle and is reduced if the adhesive force increases. The surface between the liquid and the air is called the meniscus, which can either be concave, convex or planar depending on the surface tension. The total capillary force is the sum of the surface tension force ( $F_S$ ) and the pressure force ( $F_P$ ) during the interactions of fluids and solids [13; 14]. Equation 5 can be rewritten as equation 6.

$$F_c = F_P + F_S \quad (5)$$

$$F_c = A * P_c + L * \gamma * \sin(\theta) \quad (6)$$

## 2.2 Wet adhesion in tree frogs

The mucus and the toe pads of the tree frog have been studied in order to obtain a better understanding of this animal and its capabilities of wet adhesion [5; 15]. The studies established the mucus parameters for tree frog adhesion, the physical changes in respect to the mucus during the movement of the frog, and potential models which can be used to simulate the capillary force of the tree frog.

The mucus is a water-based solution produced by the tree frog primarily to retain moisture to enable skin breathing and to regulate temperature [16; 17]. The mucus may have other purposes such as being used as an adhesive layer for wet adhesion to increase mobility. The mucus has been studied before to get a better understanding of its notable parameters for wet adhesive functions. The mucus contains surfactant molecules which increases the wettability and reduces the surface tension to achieve a contact angle of less than  $10^\circ$  on hydrophobic and hydrophilic surfaces [5; 18]. The surface tension of the mucus has not been studied but it can be considered low relative to water due to its high wettability. A low surface tension would translate to a low surface tension force term of the capillary force, meaning the pressure force term would be the dominant term.

As the tree frog moves around and attaches itself to different surfaces, the frog releases mucus at the toe pads, surrounding the bottom of the pad fully with a wedge thickness of  $5 \mu\text{m}$  to  $10 \mu\text{m}$  and an unknown meniscus height and curvature [19]. Furthermore, studies have shown that adding a surfactant to the tree frogs toe pads impaired their ability to stick to walls, suggesting that the capillary force is indeed used for their wet adhesion [5].

Following equation 6 from the theory of the capillary force explained in section 2.1, in order to determine the capillary force, the effective radius of the meniscus and the contact area have to be determined in the case of the tree frog. Due to the curved shape of the toe pad, the capillary force can best be approximated as the capillary force between a plane and a sphere, see figure 2 [5; 13]. This is only a rough approximation as the toe pad is not a rigid sphere.

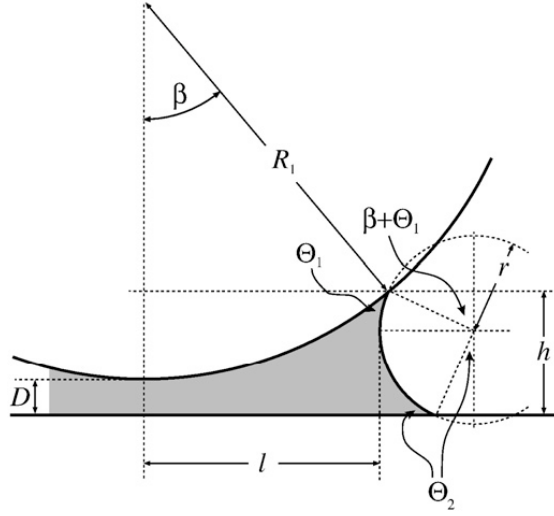


Figure 2: Schematic of the liquid bridge between a plane and a sphere.

$$F_c = 2 * \gamma * \pi * l - A * P_c \quad (7)$$

$$A = \pi * l^2 \quad (8)$$

$$l = R_1 * \sin(\beta) - r * (1 - \sin(\Theta_1 + \beta)) \quad (9)$$

$$r = \frac{R_1 * (1 - \cos(\beta)) + D}{2 * c} \quad (10)$$

$$c = \frac{\cos(\Theta_1 + \beta) + \cos(\Theta_2)}{2} \quad (11)$$

Furthermore, due to the low contact angle and low surface tension of the mucus, the capillary force can be further estimated as the pressure force multiplied by the effective area. By omitting the surface tension force, the calculations are greatly simplified and there will be no need for a camera to measure the meniscus radius and contact angles [5; 13].

$$F_c = F_P = A * P_c \quad (12)$$

## 3 Concept development

The objective is to determine the capillary force of the tree frog, which according to section 2.1, requires three sets of parameters to be measured: meniscus parameters (effective length and contact angle), area and either force or pressure. The meniscus parameters or meniscus shape will determine the surface tension force term, and the area with the pressure will determine the pressure force term. These two terms sum up to the capillary force. The capillary force can also be directly measured, but the surface tension force and pressure force terms will still be necessary to verify the results from the system with the theoretical calculations, in which case the meniscus shape and area are still necessary. To fulfil this objective, the design procedure of the system will follow a generic process: requirements definition, concept creation, concept selection, system construction and testing.

### 3.1 List of requirements

The first step into designing a new system is to define a list of requirements. This list is created through common requirements to measure any parameter (precision, speed, cost), through special factors regarding the test subjects, such as tree frogs (does not harm the subject, is not intrusive) but also through the limitations created by other components (does not obstruct components). Table 1 lists the requirements in order of importance to prioritise satisfying the critical requirements. The requirements were not given a weight factor due to the relatively short list, the preference of a concept in relation to the requirements can be shortly discussed.

The most important requirement is the precision of the measurement as the capillary force needs to be precisely measured to argue its importance. It is also important that the system should not harm the tree frog, otherwise an existing device can be used instead. For a more straightforward objective, harming the frog is considered synonymous to requiring a static target, as attaching an animal in place can be considered harming it. The system cannot be intrusive to the mucus as this will affect the mucus shape and therefore change the capillary force, which could invalidate the results if not taken correctly into account. The system should be responsive enough to measure the capillary force for the time a frog stays still on the system but it would be ideal if the system could be responsive enough to measure the capillary force during the formation and breaking of the adhesive contact. The components should obstruct the least amount of views around the substrate to allow space for other necessary components, but as there are multiple ways to place the components, it should not be an issue if they are somewhat obstructive. The concept should not be affected by the rotations of the system, which means the concept still functions properly when the system is rotated. A system that could rotate would allow future experiments at different angles, however different variations can be build, or calculations can be updated to compromise for the lack of this requirement. As the substrate will be used as a platform for the frog, limitations regarding the properties of the substrate should be considered, such as its transparency. A substrate can always be designed to try to fulfill these limitations. Finally the least important requirement is the cost, as long as these costs aren't unreasonable.

Classifiers were used to give an objective result of the concept. There are two types of classifier and each classifier has four levels of satisfaction to the requirements. "Yes/no" classifiers are used to identify if the concept follows the requirement. In some cases it may not fully comply or fully oppose the requirement, in which case, explanations are included to place the concept into one of the four levels of satisfaction. Value classifiers are used to identify the concept between four different ranges of numbers. The numbers are estimated to give a better idea of when a

requirement is more or less followed.

Requirements (by importance)	Classifier
Precise measurement	Value
Does not harm the tree frog	Yes/no
Intrusive to the mucus	Yes/no
Responsive and continuous measurement	Value
Obstruct views (side and bottom)	Yes/no
Affected by the rotations of the whole system	Yes/no
Limitations related to the substrate	Yes/no
Cost	Value

Table 1: List of requirements from higher importance to lower importance

## 3.2 Concept Creation

The next step into designing a new system is to create a certain number of concepts. For the measurement of each of the three parameters (meniscus shape, area and force/pressure), several concepts were created, some of which can be used to measure multiple of the three parameters. Each concept was created through brainstorm sessions and online research. In this stage any idea was kept if it can physically work, even if it is not fully proven yet. The concepts were then compared with each other using a decision matrix. The decision matrix helps select the most appropriate concept by giving a clear overview of how well concepts follow the requirements defined previously.

### 3.2.1 Meniscus shape

The mucus surrounds the toe pads creating the meniscus shape, but the parameters that define the meniscus can be obtained from the two dimensional cross section of the mucus viewed from the side as explained in section 2.2. This limits the possible concepts, so the optimal method to measure the meniscus shape is through an external video camera. There are two different ways to capture a video, primarily with the use of a visible light camera and secondly with the use of a thermal camera.

The visible light camera is one of the more versatile options to measure both the meniscus contact angle and area. A back light can also be added to increase the contrast between the object and the background. Although adding a back light increases the amount of components on the system, the results of the measurement will be more precise. Cameras can achieve high resolutions and high frame rates for a relatively low cost [20; 21].

The thermal camera measures the change in temperature instead of the change in light and colour. This is plausible as the temperature of the mucus is different than that of the ambient air. Much like the camera, the thermal camera can capture the meniscus contact angle and area through the temperature contrast between the object and the background. However, due to several differences, including a lower relevance of thermal imaging compared to visible light imaging, it may cost more to get an equal resolution and frame rate. Furthermore due to the constant heat transfer from hot object to cold ones, the barrier between the object and the background may be imprecise lowering the precision of the method [22–24].

### 3.2.2 Area

The area refers to the contact area between the mucus surrounding the toe pad and the surface the mucus is interacting with, as explained in section 2.2. It can be measured similarly to the meniscus shape as it is a two dimensional image, meaning a video camera and a thermal camera are possible concepts. Other additional possible concepts includes the area scanner and the tactile sensor.

The camera concepts works similarly for the contact area as it does for the meniscus shape but adds an additional restriction to the design of the system. The contact area is measured from the bottom of the toe pad, which would be interacting with a physical object, the substrate. This substrate would be in between the mucus and the camera, which interferes with what the camera can observe. In case of a video camera, the substrate would have to be transparent to let the light and colour through. In case of a thermal camera, the substrate will have to be thin and thermally conductive to allow for an effective heat transfer.

The contact area can also be measured through an area scanner which works similarly to a video camera but simplifies area measurement in exchange for a smaller focal length. The area scanner, similarly to the camera, measures the area by using light and colour contrast between the object and the background. The major difference is the lack of lenses which requires the area scanner to be placed close to the object. The area scanner costs less than the video camera but also has a lower resolution and frame rate [25; 26].

The contact area can also be measured using a tactile sensor. This works differently than the other concepts as this requires contact with the object. The pressure provided by the object on the surface of the tactile sensor will project the area. This reduces the precision in area measurement but enables the possibility to measure the pressure as well as the area simultaneously. As the tactile sensor is opaque, it cannot be combined with another area measurement method. The precision is limited in terms of its resolution but also by the object which needs to apply a minimum amount of pressure to be recorded. Furthermore, the total weight of the frog will need to be taken account as it is not part of the capillary pressure but will be measured by the sensor. The effect of gravity when the system is rotated will effect the weight of the frog applied on the sensor and should be taken into account as well. The tactile sensor seems to be a relatively cheap option but the resolution, precision and response time will be lower than some other options [27].

### 3.2.3 Force or pressure

The final component that needs to be measured is either the total capillary force or the applied pressure, as explained in section 2. The force can be measured through a force sensor, while the pressure can be measured through either a tactile sensor, a pressure sensor or a force sensor attached to a membrane. The tactile sensor is explained in the previous section and will not be discussed further. The pressure sensor can be used in two different ways which will be called the bottom configuration and the side configuration. In the bottom configuration, the entrance to the pressure sensor will remain static as the mucus is applied. In the side configuration, the entrance to the pressure sensor will move into the side of the mucus.

The pressure sensor can measure the capillary pressure inside the mucus by having the entrance to the pressure sensor come into contact with the boundary of the mucus. A micro pressure sensors has a relatively high precision, it is relatively responsive and it can be obtained at a low

cost [28]. However, in order to place the entrance to the pressure sensor on the boundary of the mucus, it will take precise movement and time. This means that not only will the frog have to be restricted but it is also likely that the meniscus geometry of the mucus will be affected by the opening of the sensor.

The pressure sensor can also measure the capillary pressure inside the mucus by having the mucus come into contact with the entrance to the sensor placed in the supportive platform. The pressure sensor will maintain the same precision, responsiveness and cost as the side configuration but the way the sensor interacts with the mucus will be simplified [28]. The entrance to the sensor will be stationary as the object moves freely until the mucus interacts with said entrance. The fact that the sensor can run continuously allows this method to work. It will be no longer necessary to move the sensor entrance in the correct position and the system will be less intrusive. The issue with this concept is that the entrance leading to the sensor will be located between the object and the substrate. The component that will connect the entrance leading to the sensor, to the sensor can potentially obstruct the view to the mucus contact area.

A force sensor can be attached to a membrane to create a pressure sensor embedded in the substrate. It would use a force sensor, which has a high precision, low cost and low responsiveness attached to the membrane of known size and parameters located in the substrate below the object. It will effectively measure the pressure similarly to the pressure sensor in the bottom configuration, so this concept should not be affected by the rotation of the system. Due to its location, it can significantly obstruct the view to the contact area of the mucus [29; 30].

The force sensor has been used before to measure the capillary force between different liquids and surfaces [7; 9]. It is usually of high precision and low cost but lacks in responsiveness. In liquid systems, the low responsiveness and the necessity to wait for an equilibrium to be achieved is not a problem as the object to be studied is controlled, however in the case of a living object this is not the case. Furthermore, the force sensor will also measure the force applied by the weight of the frog, meaning the sensor will have to be placed in a way that the weight of the frog can be ignored or the weight of the frog will have to be taken into account during calculations. The weight issue must also be taken into account during the rotation of the system [29; 30].

		Measurement Precision (est.)	Necessity of a static target	Limitations related to the substrate	Responsive and continuous measurement (est. in Hz)	Affected by the rotations of the whole system	Obstrudes side view	Obstrudes bottom view	Mucus Intrusivity	Cost (est. in euro)
	OR									
M e n i s c u s	Camera (with backlight)	As precise as the captured image, high resolution (0-50 Mp)	Does not need a static target	Works with any substrate	Continuous, speed depends on frame rate (0-1 000 000)	Needs to take into account the new shape of the mucus	Utilizes 2 sides	Does not obstruct	Not intrusive	Expensive (300->10,000)
	Thermal camera	As precise as capture image, low resolution (0-5Mp)	Does not need a static target	Works with any substrate	Continuous, speed depends on frame rate (0-100 000)	Needs to take into account the new shape of the mucus	Utilizes 1 side	Does not obstruct	Not intrusive	Very Expensive (300->15,000)
A r e a	Camera (with backlight)	As precise as the captured image, high resolution (0-50 Mp)	Does not need a static target	Needs transparent substrate	Continuous, speed depends on frame rate (0-1 000 000)	Not affected by rotations	Does not obstruct	Utilize bottom view	Not intrusive	Expensive (300->10,000)
	Areascanner	As precise as the captured image, high resolution (0-10 Mp)	Does not need a static target	Needs transparent substrate	Continuous, speed depends on frame rate (0-3500)	Not affected by rotations	Does not obstruct	Utilize bottom view	Not intrusive	Fairly Expensive (300-2000)
	Thermal camera	As precise as capture image, low resolution (0-5Mp)	Does not need a static target	Needs thin isotropic substrate	Continuous, speed depends on frame rate (0-100 000)	Not affected by rotations	Does not obstruct	Utilize bottom view	Not intrusive	Very Expensive (300->15,000)
	Tactile sensor	As precise as capture image, low resolution (0-248/cm <sup>2</sup> )	Needs time to achieve response	Needs to be placed on top of substrate	Continuous, speed depends on response time (>100)	Needs to take rotations into account	Does not obstruct	Utilize bottom view	Not intrusive	Cheap (<100)
F o r c e / P r e s s u r e	Tactile sensor	Low precision (10 <sup>-2</sup> Pa)	Needs time for the mucus to reach an equilibrium	Needs to be placed on top	Continuous, speed depends on response time (>100)	Needs to take rotations into account	Does not obstruct	Obstrudes	Not intrusive	Cheap (<100)
	Side pressure sensor	High precision (10 <sup>-1</sup> Pa)	Needs time to enter the meniscus and achieve response	Works with any substrate	Continuous, speed depends on response time (>1000)	Needs to take height difference from rotations into account	Utilizes 1 side	Does not obstruct	Intrusive	Cheap (<100)
	Bottom pressure sensor	High precision (10 <sup>-1</sup> Pa)	Needs time to achieve response	Needs tubing through substrate	Continuous, speed depends on response time (>1000)	Needs to take height difference from rotations into account	Does not obstruct	May obstruct significantly	Not intrusive	Cheap (<100)
	Force sensor attached to membrane	High precision (10 <sup>-9</sup> N)	Needs time to achieve response	Needs membrane placed in substrate	Continuous, speed depends on response time (<500)	Not affected by rotations	Does not obstruct	May obstruct significantly	Not intrusive	Cheap (<100)
	Force sensor	High precision (10 <sup>-9</sup> N)	Needs time for the mucus to reach an equilibrium	Substrate cannot be too heavy	Continuous, speed depends on response time (<500)	Needs to take rotations into account	Does not obstruct	May obstruct partially	Not intrusive	Cheap (<100)
		Goes against requirements			Complies with requirements					

Figure 3: Decision matrix for the selection of the concept

### 3.3 Concept Selection

Following the decision matrix, figure 3, the preferred concepts are further developed and sketched in order to compare them. Cameras are used to measure the meniscus shape as well as the area for both final concepts. The concepts vary in terms of the component to measure the force/pressure. As seen in figure 4, concept 1 uses a pressure sensor which is connected to the substrate through a tube and concept 2 uses a force sensor attached to a membrane, which is connected to the substrate. The force sensor decreases the visibility compared to the tube, the tube can be selected to be transparent or it can be implemented inside of the substrate. Concept 1 is selected to make it possible to measure the contact area accurately and still maintain a relatively high pressure measurement precision and response.

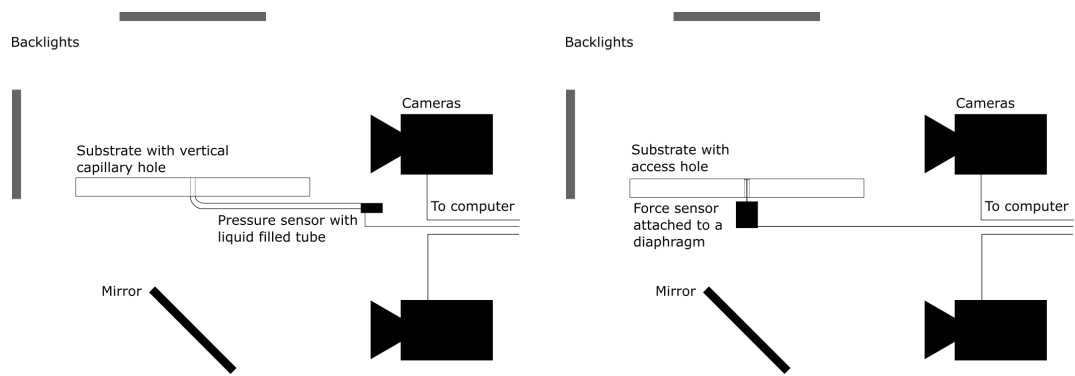


Figure 4: 2D sketch of the 2 chosen concepts from the matrix

## 4 System development for capillary pressure measurement

### 4.1 Measurement principle

The system will work based on the flow of liquid generated by the capillary pressure. The flow generated by the capillary pressure in the mucus deforms the membrane, as shown in figure 5. The deformation in the membrane is measured, which is used to calculate the flow and accordingly the unknown capillary pressure. As the system is equivalent to a RC circuit following the hydraulic-electric analogy, the flow can be expressed following equation 13 [31; 32].

$$q = C * \frac{dP}{dt} = \frac{P_c}{R} \quad (13)$$

Where  $q$  the flow rate of the liquid,  $P_c$  is the capillary pressure of the mucus,  $P$  the internal pressure of the sensor,  $C$  the hydraulic capacitance and  $R$  the hydraulic resistance. Equation 13 can be rewritten as equation 14.

$$P_c = C * R * \frac{dP}{dt} \quad (14)$$

In order to calculate the capillary pressure correctly, the hydraulic capacitance and the hydraulic resistance need to be determined or selected. The hydraulic capacitance is determined through the displaced volume of a deformable object per applied pressure. In the hydraulic chamber, the membrane is the deformable object. The hydraulic resistance is determined through the friction of a wall on a flowing liquid, which depends on the size, length and shape of the tube. In a hydraulic-electric analogy, the system is equivalent to a RC circuit with a time constant  $\tau$  which can be calculated from the total hydraulic resistance and the total hydraulic capacitance following equation 15 [32].

$$\tau = R * C \quad (15)$$

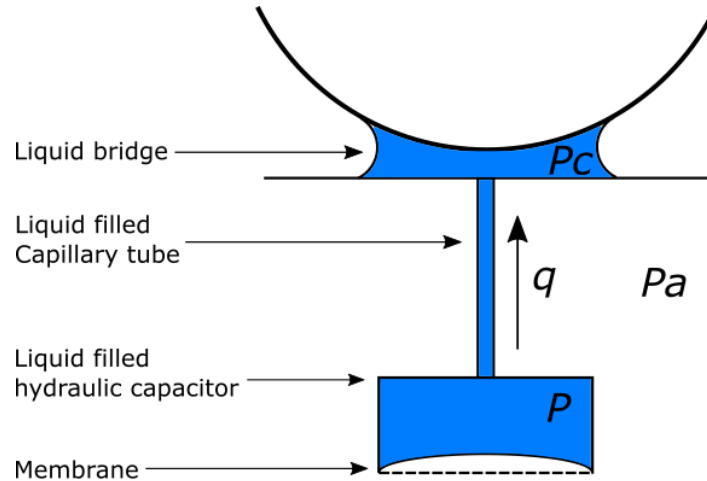


Figure 5: Sketch of the principle of measurement.  $q$  represents the flow of the liquid that moves from the higher pressure to the lower pressure.  $P_c$  represents the capillary pressure of the mucus,  $P$  represents the pressure inside the sensor and  $P_a$  represents the ambient air pressure. The dotted lines represents the membrane which moves due to the change in liquid volume in the hydraulic capacitor.

## 4.2 Component selection

Following the sketch of the conceptual system seen in figure 4, there are 5 components that need to be selected to make the system function.

- A hydraulic capacitor
- Two cameras
- A substrate with a capillary channel
- A tube to connect the substrate to the sensor
- A liquid medium

Each component will have to be selected to fulfil the design requirements but also to take into account the other components. The specifications to take into account include the optical parameters to allow for an accurate measurement of the contact area and meniscus shape, as well as the fluidic parameters to obtain a good system time constant.

### 4.2.1 Hydraulic capacitor

A commercially available pressure sensor containing a deformable membrane is used as the hydraulic capacitor due to the ease of use benefits. The membrane is instrumented such that the deformation is measured as an electrical output. The sensor needs to follow a few requirements. It must be very sensitive, i.e. it must measure a minimum pressure as small as 10 Pa, which is four orders of magnitude smaller than that of the unknown (capillary) pressure. In order to obtain such a sensitivity, the working range of the sensor has to be restricted to approximately 10 kPa, which is approximately the initial estimated value of the unknown (capillary) pressure. Owing to the ease of implementation, it is favourable if the commercially available sensor has a barbed port, a pin DIP or SIP connection and a digital I2C or SPI connection. The obtained pressure sensor is the SSCDRRV100MGSA3 by Honeywell [28]. An Arduino was used to read the information sent from the sensor and send that data as readable numbers to the computer. This sensor works at the supply of 3.3 V DC meaning the arduino used should apply 3.3 V. The arduino DUE is selected to accompany the sensor as it is a versatile board which applies 3.3 V [33].

The deformation of the membrane caused by a change in liquid volume is related to the physical property of the hydraulic capacitance  $C$ . The hydraulic capacitance can be estimated from the membranes shape, dimensions and material properties. The membrane can either be circular or quadratic, which effects the capacitance by the shape factor  $S$ . The shape of the membrane of the SSCDRRV100MGSA3 sensor is quadratic. The capacitance of a quadratic membrane is given by equations 16 and 17 [32].

$$C = \frac{S * a^6 * (1 - p^2)}{t^3 * E} \quad (16)$$

$$S = \frac{1}{66} * \left(\frac{8}{15}\right)^2 \quad (17)$$

In order to estimate the range of the hydraulic capacitance, the width and thickness of the membrane from an opened sensor were measured with the help of a Keyence Optical Measurement System. As seen in figure 6, the membrane has a width of  $a \approx 0.9198$  mm and a thickness of  $t \approx 9.1$   $\mu$ m.  $p$  is the Poisson's ratio and  $E$  is the elastic modulus of the material of the membrane. The material used in these types of sensors is silicon, therefore the Poisson's ratio and elastic modulus are estimated from literature as:  $p = [0.25 - 0.3]$  and  $E = [110 - 180]$  GPa [28; 34]. The

hydraulic capacitance of the sensor is estimated to be between  $C = [1.751 * 10^{-17} - 2.952 * 10^{-17}] \text{ m}^3 \text{ Pa}^{-1}$  or  $C = [1.751 * 10^{-2} - 2.952 * 10^{-2}] \text{ pL Pa}^{-1}$ .

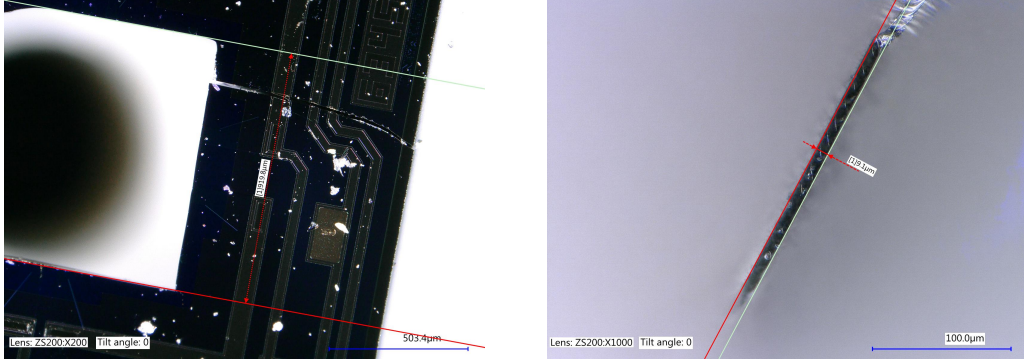


Figure 6: Approximate measurements of the membrane width  $a$  (left image) and thickness  $t$  (right image) obtained through the optical measurement system.

#### 4.2.2 Cameras

The cameras will be used to capture the shape and contact area of the meniscus. They will be positioned to capture images below and to the side of the substrate. The camera used are a set of Mikrotron MC1362 (1280 px  $\times$  1024 px, max 500 fps) with an Epix PIXCI-E8 frame grabber. The cameras have the Nikkor 105 mm AF-D lens in combination with a +5 Mareumi close-up lens and a 21.5 mm extension tube attached to it for a practical focal length. The cameras will be positioned on the railings such that the drop is in the correct focal length.

#### 4.2.3 Substrate

The substrate is used as the solid surface the frog will walk on and it will contain a capillary channel filled with a liquid medium connected to the hydraulic capacitor. The substrate is designed to retain the liquid medium, even against gravity, by using the effect of the capillary action from the surface tension of the liquid [35]. The size of the opening leading to the sensor must be small enough for the surface tension force to overcome the weight of the liquid column, which can be calculated using equation 18. The equation takes into account the surface tension  $\gamma$ , the density  $D$  of the liquid, the gravitational constant  $g$  and the length of the channel  $L$  to determine the maximum radius  $R$  of the channel such that the liquid will not flow out.

$$R = \frac{2 * \gamma}{g * L * D} \quad (18)$$

The substrate will largely determine the time constant as it behaves as a hydraulic resistor. The substrate would have to be made from a sufficiently rigid material in order to have a hydraulic capacitance that can be considered insignificant compared to the hydraulic capacitance of the membrane of the hydraulic capacitor [31]. The hydraulic capacitance of the substrate would then be ignored to simplify calculations. The hydraulic resistance of the substrate is a major factor for the time constant due to how small the capillary channel is. The resistance depends on the shape of the channel and its size; the resistance can be calculated with equation 19 in the case of a channel having a quadratic cross section, where the height is equal to the width. The viscosity

of the fluid  $v$ , the length of the channel  $L$  and the width of the channel  $W$  are the necessary parameters [36].

$$R \approx \frac{32 * v * L}{W^4} \quad (19)$$

As discussed previously, the substrate would include a capillary channel, which can be implemented in multiple ways. Figure 7 shows the different options of implementing the channel, which can be achieved using different methods. Option 1 is a simple solution as the channel can be drilled straight through the substrate, but the connection to the sensor can moderately obstruct the view of the contact area. Furthermore, it is difficult to drill holes of less than  $100 \mu\text{m}$  in diameter without access to high-precision equipment. Option 2 can also be produced by precise drilling, or other manufacturing processes, whilst not obstructing the view of the contact area as much as Option 1. However, Option 3 also does not obstruct the view of the contact area as much as Option 1 and, through online research, is seemingly the most accessible due to the Lab-on-a-Chip technology used by fluidic engineers. They are produced as off-the-shelf designs using different manufacturing processes such as injection moulding. Due to the simplicity of a precise and accessible option, where the system will be initially working as a proof of concept, Option 3 is favoured. The selected substrate is the fluidic 143 chip from Microfluidic-Chipshop with a squared channel of  $20 \mu\text{m}$  wide, with a channel length of  $58.5 \text{ mm}$  and an opening diameter of  $50 \mu\text{m}$ . The fluidic 143 chip comes in two materials: PMMA and Topas. The chosen material is Topas as it is less water absorbent and approximately as hard as PMMA at room temperature. Both of these materials are considered sufficiently rigid that the hydraulic capacitance can be ignored [31; 37].

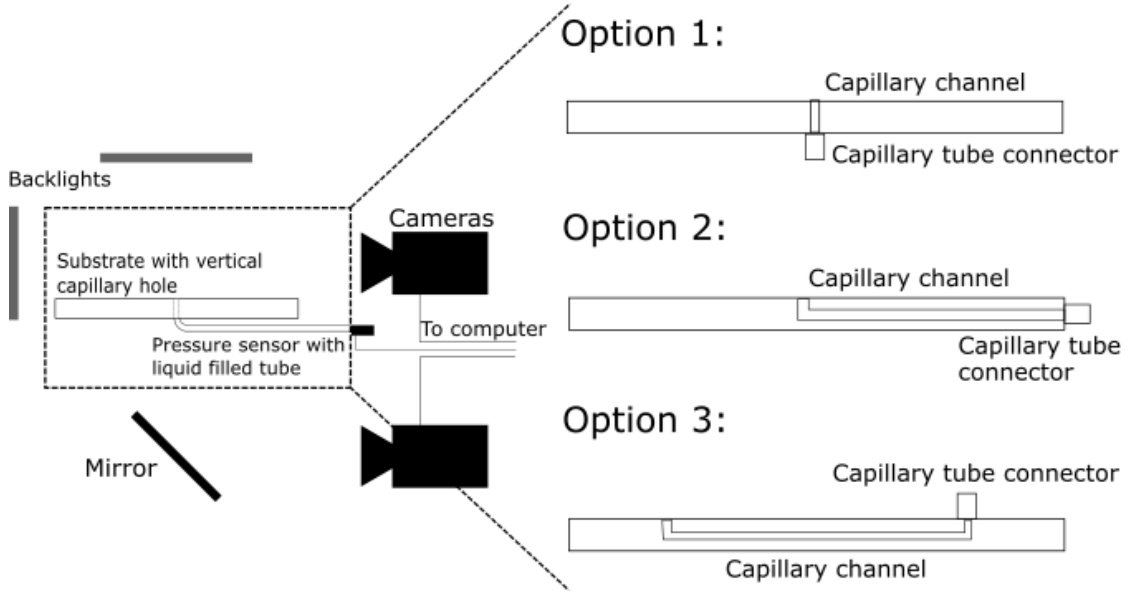


Figure 7: Sketch of the 3 possible ways to include a capillary channel in the substrate.

#### 4.2.4 Tube

The tube will be used to connect the substrate to the pressure sensor, and similarly to the substrate and hydraulic capacitor, the tube will be filled with a liquid medium. As the substrate

will have a set fluidic resistance, the tubes internal diameter and length will be selected to compensate for any lack of fluidic resistance of the substrate. Similarly to the substrate, the capacitance will have to remain as low as possible, which means that the tube will have to be relatively hard. PEEK tubes are some of the hardest, flexible tube used by fluidic engineers, which can also have some of the smallest internal diameters; they should serve as great options to increase the total resistance [36; 38; 39]. A PEEK tube of inner diameter (ID) 25  $\mu\text{m}$  is going to be used to increase the fluidic resistance, however the outer diameter (OD) is 360  $\mu\text{m}$  large, meaning adaptors will be necessary to connect the tube to the substrate and the pressure sensor [40].

$$R \approx \frac{8 * v * L}{\pi * R^4} \quad (20)$$

The easiest way to adapt tube sizes without any leak is with the use of sleeves and soft wall tubing, such as silicone, of a smaller ID. Sleeves and soft walled tubes can expand to adjust their diameters while maintaining the required pressure onto the wall to increase friction and reduce the risk of leakage. The sensor contains a barbed port with an OD of 1.6 mm, so a silicone tube with an ID of 1.5 mm is required to connect the PEEK tube to the sensor. An additional sleeve of ID 0.015 mm is required to increase the OD of the PEEK tube to 1.6 mm. The substrate will have an olive fluidic port with an OD of 2 mm, so the same tube that is being used to connect the PEEK tube to the sensor can be used to connect the olive port to the PEEK tube. The connections of the tubes and ports can be seen in figure 8.

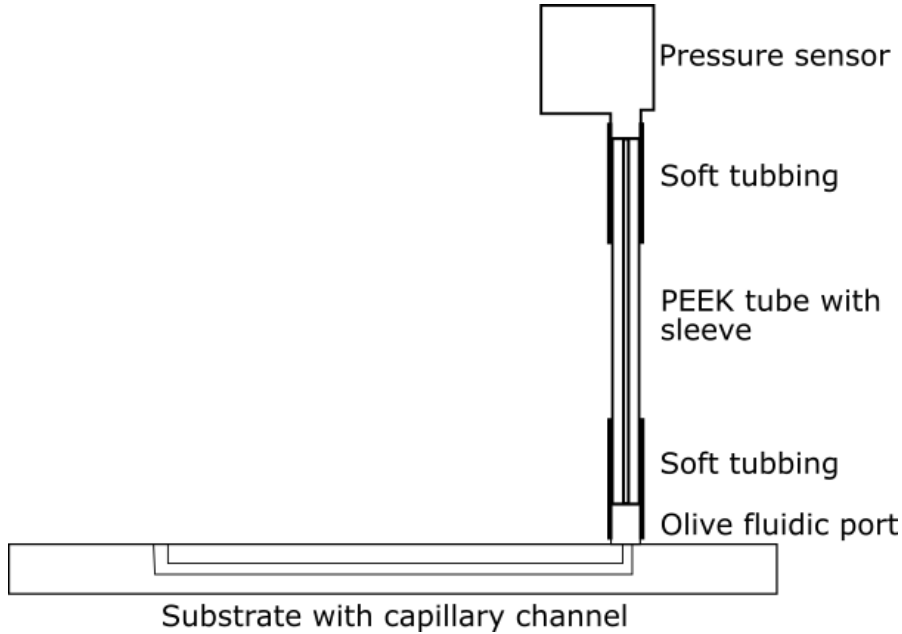


Figure 8: Schematic of how the PEEK tube will be connected to the sensor and to the substrate.

#### 4.2.5 Liquid medium

The liquid medium will fill the substrate, the tube and the pressure sensor to allow the liquid flow to be detected by the hydraulic capacitor. If the medium is a compressible fluid, such as air, the system will respond too slowly to the changes in pressure as the fluid will have to compress

to its smallest volume at pressure first, i.e. the fluidic capacitance will be too large. For this reason, a liquid medium is used, which is less compressible. The liquid will obstruct the view of the contact area so it must remain transparent, preferably with an equal refraction index to the substrate. The liquid may not contaminate the mucus of the frog or damage the materials in contact (substrate, tube and sensor). Water will be the initial choice as its properties are well known and it will not damage the components, but a more appropriate liquid medium can be selected in the future after performing additional research [28; 40; 41].

#### 4.2.6 Additional components

There are other necessary components which need to be added to monitor and test the final system but do not take part in the principal workings of the system. A DHT 22 Joy-IT thermometer is added to measure the temperature near the liquid channel. If the temperature of the liquid channel changes during measurements, the volume and the pressure will change. As the system functions with small volumes of liquid, these temperature changes can affect the measurements significantly. In order to apply a liquid meniscus to parallel the mucus of the frog and verify the capillary force measured by the system, a mobile force sensor system is implemented. It includes a metallic sphere with a known radius, which is attached to a Futek lsb200 force sensor. The force sensor is connected to a Thorlabs three-axis motorized stage which can move in all three directions [42–44].

### 4.3 System assembly

The selected components need to be assembled into a system in a working manner. The cameras will have to be correctly aligned with the opening leading to the sensor to record the values with the best precision. The sensor will have to be placed at such a position that the tubes have a straight path and the required length determined by the calculated hydraulic resistance. Sufficient space must be reserved to add any additional components that cannot be placed far away from the system, such as the additional components mentioned in section 4.2.6. All the structural components must be added to fix the components in the correct position and allow for any components that need to be able to move to maintain the high precision. Solidworks is used to create the 3D model to visualize how each components can be placed and to determine the length of any structural components that need to be produced.

As seen in Figure 9, the system will be placed on a table with a hole in the center. The hole is to allow space for the lower camera while allowing the system to rest on the table. Placing the bottom camera vertically will simplify the design compared to the concept shown in Figure 4 and remove the need to use and align a mirror. The system will rest on the table to reduce vibrations and materials. The frames are placed directly on the table to support the components; the frames surrounding the bottom camera are of two different heights. The taller frames are used to give the substrate enough height to align the opening of the pressure system with the center of the side camera. The smaller frames provides space for the side camera to be placed as close to the substrate as necessary. To maintain the structural integrity of the plates used to place the components, they are connected through a bridge on the side of the light source.

The components are placed in a condensed manner around the opening to the sensor, which will be considered the center of the system. The opening leading to the sensor is located at the correct focal distance away from the cameras. The cameras can be moved alongside and across the railings for better precision. The object, in this case the metallic sphere, can be moved using

the XYZ-stage to the appropriate location. The substrate is secured using a thin rubber-metal plate screwed into the substrate holder. The substrate holder has a large enough hole at the bottom to allow the camera to correctly view the bottom of the substrate. The substrate holder is slightly larger than the substrate to allow the centering of either of the four channel openings. This allows a different channel to be used if something happens to one of the channels or if the channels are filled with different liquids for testing purposes. A thermometer is placed near the substrate to measure the change in temperature as this affects the volume and pressure of the liquid inside the channel. The pressure sensor is placed vertically to reduce severe bending of the tubes connecting the sensor to the substrate. The pressure sensor, thermometer and Arduino are placed close the one another to reduce cable lengths. These objects placed vertically may increase vibrations due to the height of the vertical platform. These vibrations can affect the measurements, as seen when moving the vertical platform, changes in pressure were measured.

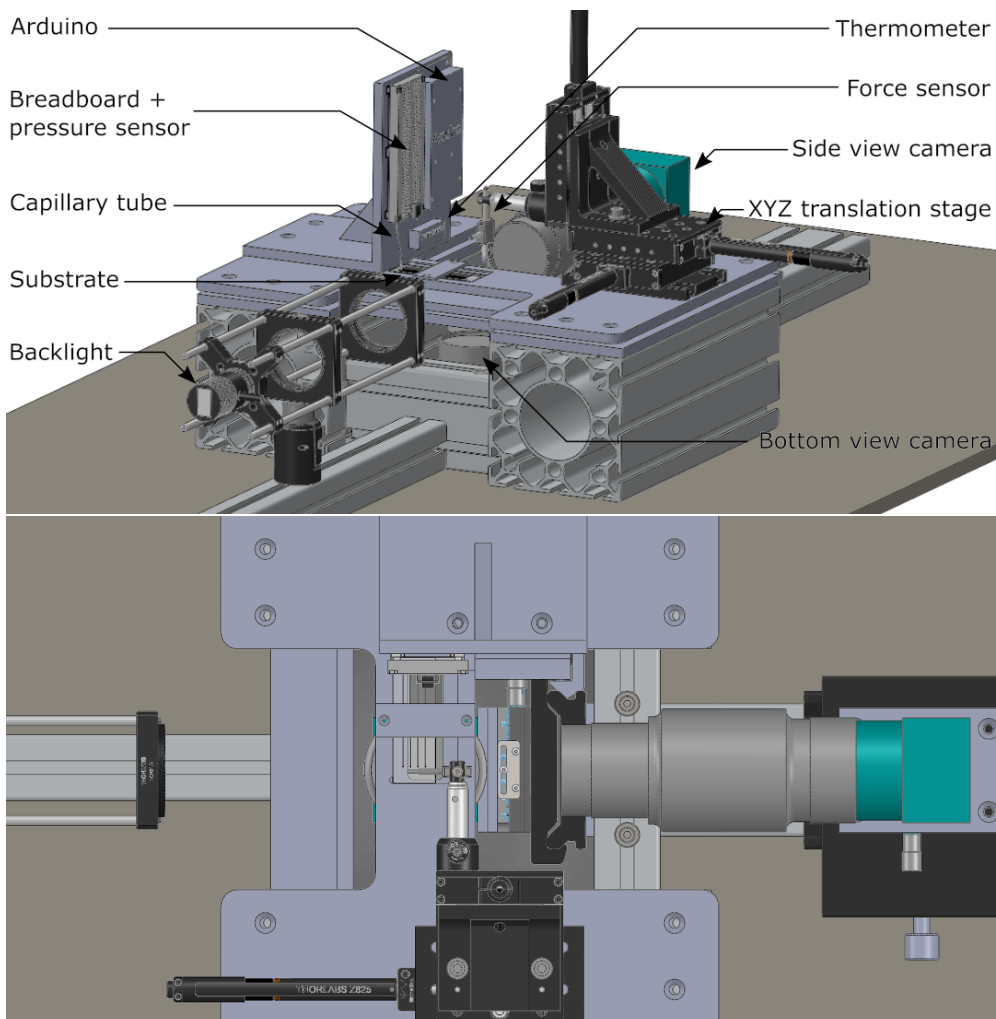


Figure 9: Overview model of the final system with the placement of the key components. The orthogonal view (top) shows the placement of all the components and the top view (bottom) shows the alignment of the components around the substrate.

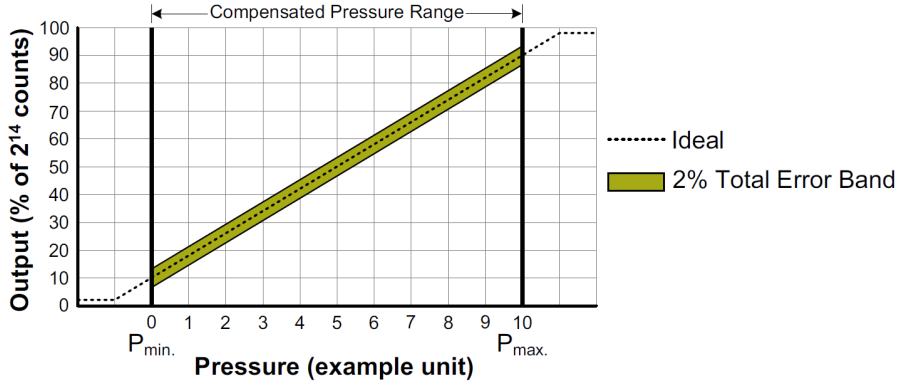
## 5 System functionality measurements

In order to verify the functionality of the components as well as the system as a whole, multiple experiments will have to be performed. First of all, the pressure measurement accuracy, range and precision needs to be verified. This means the hydraulic capacitor needs to be calibrated and tested across the expected range. A noise analysis is also performed to verify if the noise will not overshadow the measured value. Finally, a proof of concept is necessary to support the creation of this system; preferably using the components akin to the final design.

### 5.1 Calibrating and verifying the working range of the pressure sensor used as a hydraulic capacitor

The pressure sensor purchased to be used as a hydraulic capacitor needs to be calibrated and tested in order to function properly in the system. Each pressure sensor can behave slightly differently, the data output will not be the exact same across multiple sensors, which is why they need to be calibrated to a known value pressure source before use. The sensor is calibrated using equation 22 with the output values being the bit data the sensor sends to the Arduino and the pressure values the respective pressure translated from the bits. The calibration can be done with either 2-points, 3-points or more points but in this case the 2-points method was sufficient due to the linearity of the sensor in the necessary pressure range, as seen in figure 10 [28]. As the calibration determines the slope of the system, an auto-zero function can be added to measure a relative change in pressure instead of the absolute pressure. This is useful in order to ignore any pressure applied by unwanted liquid, such as in the connecting tubes; however it may make it difficult to notice when the saturation level, the pressure at which the sensor does not remain linear, is reached.

Digital Versions



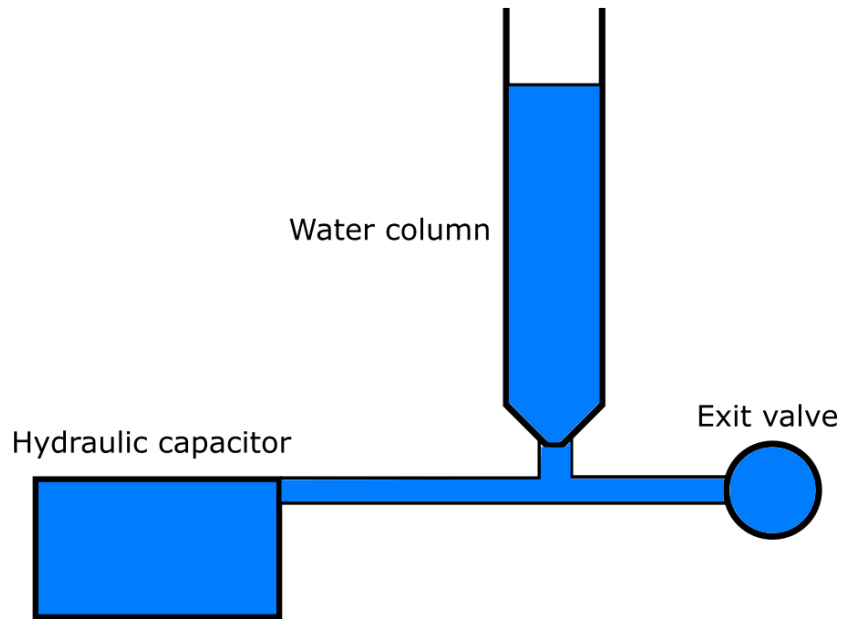
$$\text{Output (\% of } 2^{14} \text{ counts)} = \frac{80\%}{P_{\max.} - P_{\min.}} \times (\text{Pressure}_{\text{applied}} - P_{\min.}) + 10\%$$

Figure 10: Pressure measurement and linearity system of the digital pressure sensor obtained from the manufacturers documentation [28].

$$\text{Pressure} = \frac{(\text{Output} - \text{Output}_{\min}) * (\text{Pressure}_{\max} - \text{Pressure}_{\min})}{(\text{Output}_{\max} - \text{Output}_{\min})} + \text{Pressure}_{\max} \quad (21)$$

In order to verify if the pressure sensor functions as expected, the same set of experiments to calibrate the sensor has been done. The verification process is to determine if the sensor is indeed linear during the whole expected pressure range, which in this case is 0 kPa to 10 kPa. There are two methods to calibrate and verify the pressure sensor, which can be seen in Figure 11: the hydro column method and the air-pressure source method. The air pressure source method was used to calibrate the sensor and the hydro column method was used to verify the calibration. The air-pressure source method uses controlled air pressure which passes through an already calibrated manometer, then to an air-to-water converter and finally to the sensor. The main issues in this case is that the sensor is calibrated as precise as the manometer allows, if the air pressure source does not vary too much. The hydro column method has the sensor connected to a water column of known height which applies a set pressure. The available water column range to verify the sensor is 0 cm to 120 cm which equates to approximately 0 kPa to 12 kPa. The main issues from using this method includes the imprecision caused by human error when setting the height. A technique used to maintain a high precision is setting the height by removing water with the use of a valve.

### Water column setup:



### Air pressure source setup:

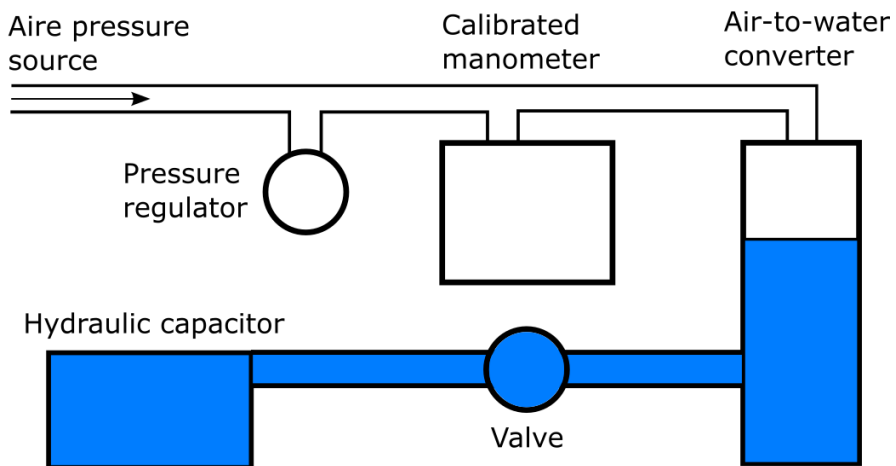


Figure 11: Experimental setups to apply a known hydraulic pressure to the sensor. The water column experiment (top) uses a water column of more than 120cm to apply pressure and the air pressure source experiment (bottom) uses air pressure connected to an air-to-water converter to apply pressure.

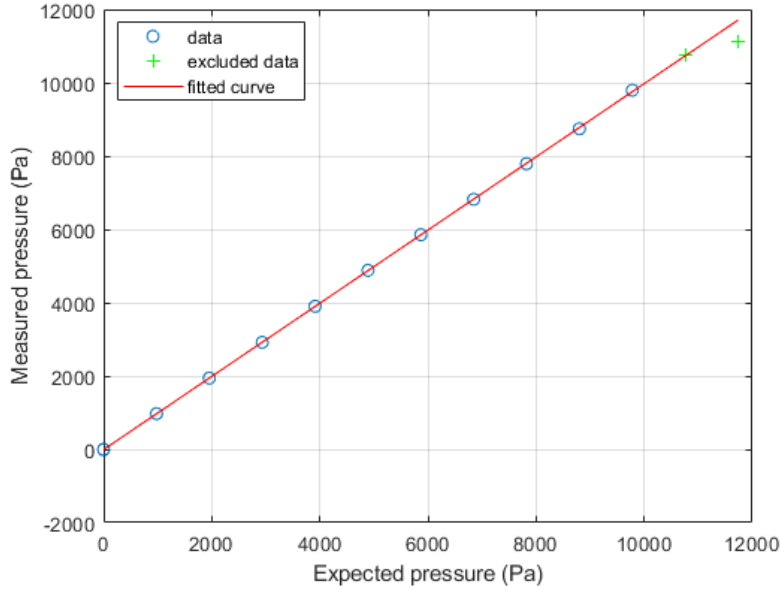


Figure 12: Pressure measured by the pressure sensor vs. the applied pressure. Data was obtained using the water column setup.

$$P_{measured} = 0.9981 * P_{expected} - 8.147 \text{ Pa} \quad (22)$$

The calibration succeeded following the results of both the hydro column method and the air pressure source method. By verifying the results of the hydro column method of 0 cm to 120 cm with 10 cm intervals, the sensor does indeed remain linear up to approximately 10 kPa to 11 kPa where it starts to curve as it tends to 12 kPa.

## 5.2 Sensor noise evaluation

The noise of the pressure sensor is essential in determining the accuracy of the sensor during general pressure measurements [28]. In order to determine the change in accuracy across different pressure ranges, data was acquired using the air pressure source method. During the measurements, a linearly decreasing trend would generally occur when applying pressure, which varied between  $-0.03 \text{ Pa/s}$  to  $-0.07 \text{ Pa/s}$ , with the steeper rates occurring at a higher applied pressure. A linear detrending algorithm is applied on each of the data to remove the drift as this is independent from the sensor noise.

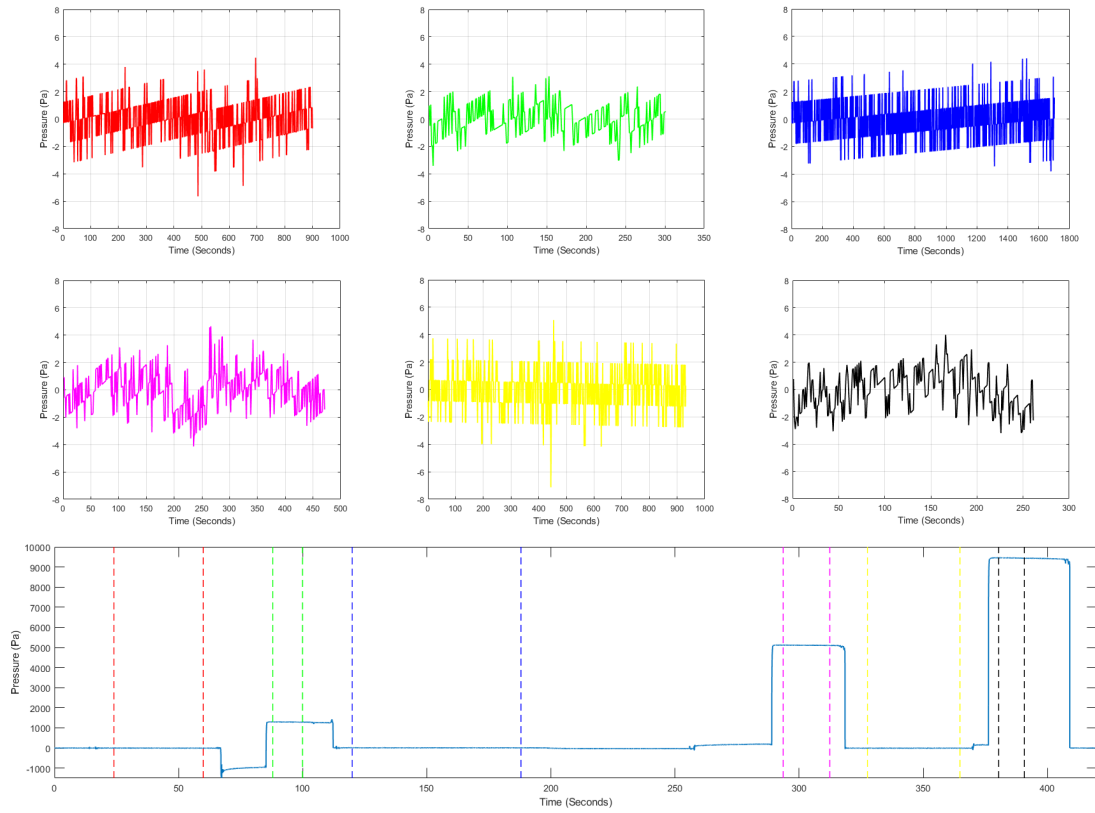


Figure 13: The data obtained during a pressure measurement experiment used to determine the noise of the sensor. The magnification of each section is shown in the appropriately coloured graphs. Each section has also been through a linear detrend function.

	Range (Pa)	Standard deviation (Pa)
System at rest prior to 1 kPa	10.121	1.355
System at 1 kPa	6.536	1.152
System at rest prior to 1 kPa	8.217	1.291
System at 5 kPa	8.785	1.445
System at rest prior to 1 kPa	12.196	1.481
System at 9 kPa	7.212	1.457

Table 2: Range and standard deviation to the mean of the pressure measured by the sensor. When at rest, no pressure is applied; at higher pressure, a pressure of 1 kPa, 5 kPa and 9 kPa were applied respectively.

The noise produced by the sensor remains consistent throughout the change of pressure. This is expected as the sensor noise is independent to the measured pressure. The noise produced by the sensor is approximately  $\pm 6$  Pa. For the final system, a filter can be applied to omit this noise.

### 5.3 Evaluating the hydraulic capacitance

In order to experimentally determine the time constant, the sensor should be connected to a capillary tube of known hydraulic resistance. For this experiment, a capillary tube of  $ID = 254 \mu\text{m}$  and  $L = 136 \text{ mm}$  was used, meaning the hydraulic resistance is  $R = 1.33 * 10^{12} \text{ Pa s m}^{-3}$ . The simple hydraulic resistance and hydraulic capacitor circuit is filled with water and a known pressure is applied instantly via opening the valve using the air pressure source setup. The progressive change in the pressure across the membrane should follow equation 23, with  $P_0$  as the known applied pressure,  $\tau$  as the time constant and  $c$  as the offset or y-intercept. The time constant is evaluated by fitting the experimental data using equation 23, from which the experimental hydraulic capacitance can be obtained through equation 24. The experimental hydraulic capacitance and time constant should be equal to their theoretical values.

$$P = P_0 * e^{-t/\tau} + c \quad (23)$$

$$\tau = R * C \quad (24)$$

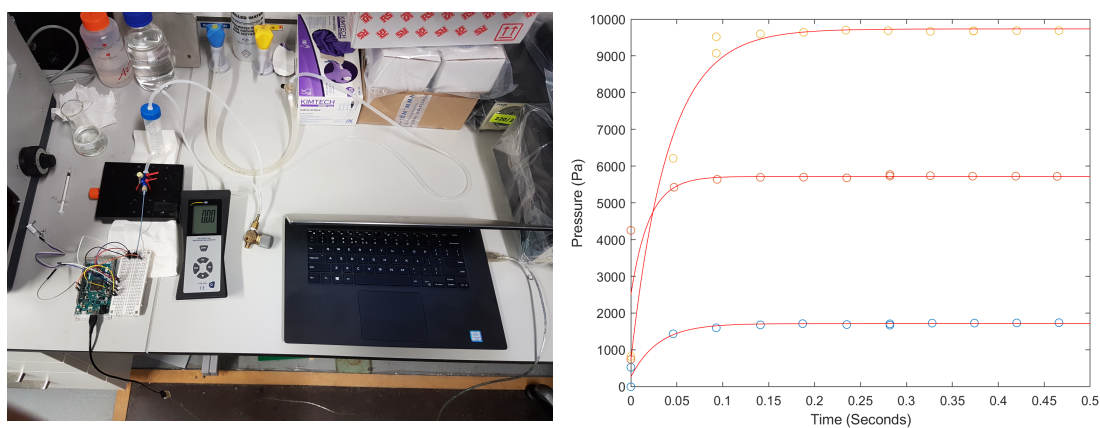


Figure 14: Air pressure source setup (left) and result (right) in order to determine the time constant of the setup and the hydraulic capacitance of the sensor.

		Time constant (s)	Hydraulic capacitance ( $\text{m}^3 \text{ Pa}^{-1}$ )
Experimental	At 1.5 kPa	2.95e-02	2.216e-14
	At 5 kPa	2.00e-02	2.502e-14
	At 9 kPa	4.05e-02	3.042e-14
	Mean	3.000e-02	2.254e-14
	Standard deviation	1.030e-02	7.706e-15
Theoretical	Mean	3.006e-05	2.258e-17
	Standard deviation	4.638e-06	3.484e-18

Table 3: Time constant and hydraulic capacitance obtained during the experiment compared to the expected calculated outcome

The experimental hydraulic capacitance was found to be around three orders of magnitude larger than the theoretical hydraulic capacitance. The larger hydraulic capacitance suggests the overall system is more deformable compared to the deformability of the hydraulic capacitor. The experiment was done multiple times to review possible sources of issue. The main cause of the extra deformability prior to the results seen in table 3 was from the use of tubing that were too soft. The same issue can still be present here in the tubing connections or the PEEK tubes. Reviewing and selecting better tubing and connectors can reduce the overall hydraulic capacitance. There are still other additional issues that can increase the deformability or measurement inaccuracies. Air bubbles are a source of deformability due to the compressible gas; even when reducing air bubbles, such as by using degassed water, it may help to include methods to verify if there are any air bubbles in the system [31; 32]. Vibrations may also be a current source of inaccuracy, by greatly reducing the vibrations through fixating the valve to a heavy object, it was easier to get values out of the data. The lack of data points also contributes to a relatively inaccurate result, which can be solved by either increasing the time constant using a longer/narrower tube (higher resistance) or by more importantly increasing the sampling frequency. The experimental hydraulic capacitance is much closer to the expected value compared to the initial tests, however there still seems to be some issues regarding the tubing, the air bubbles, the vibrations and the sampling rate that would help verify the hydraulic capacitance.

#### 5.4 Additional support for the concept

Due to time constraints, it will not be possible to use the full system to fully compare the capillary force using the force sensor, pressure sensor and shape analysis. In order to support the continuation of the system, a simplified version of the system experiment was done. A simple drop of water will be used as the source of capillary pressure instead of a capillary bridge. The capillary pressure measured by the pressure sensor will be compared to the expected capillary pressure determined through shape analysis instead of comparing the capillary force of all three methods. To do this, a simple drop is placed directly on the tip of the sensor, which according to 4.1, should apply a pressure equal to the sum of the capillary pressure applied by the internal pressure difference, equation 25, and the hydrostatic pressure applied by the weight of the water, equation 26.

$$P_c = \gamma * \left( \frac{2}{R} \right) = 72.8 * 10^{-3} * \left( \frac{2}{7.5 * 10^{-4}} \right) \approx 195.3 \text{ Pa} \quad (25)$$

$$P_h = \rho * g * H = 997 * 9.8 * 1.1 * 10^{-3} \approx 10.3 \text{ Pa} \quad (26)$$

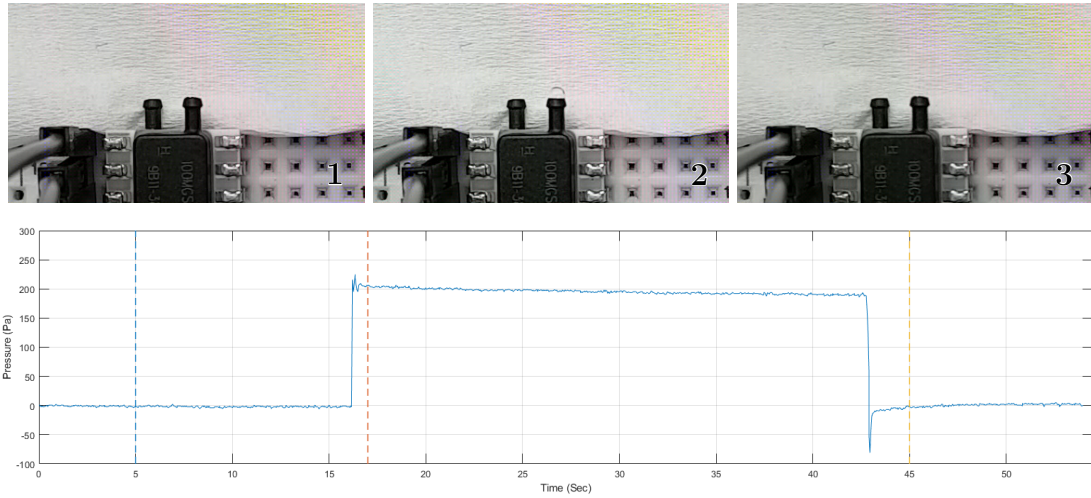


Figure 15: The data obtained when testing the capillary pressure measurement of a Sessile drop on the pressure sensor. Each of the three frames taken from the video is placed in the timeline to determine the pressure measured by the sensor. The first frame is taken at the blue timestamp, the second frame at the red timestamp and the third frame at the yellow timestamp.

By using pixel measurements on frame two in Figure 15, the bubble is measured to have a horizontal diameter of 1.5 mm and a height of 1.1 mm, the resulting capillary pressure and hydrostatic pressure are calculated to be 195.3 Pa and 10.3 Pa respectively. As seen in the pressure data in Figure 15, when the drop is applied on the sensor (frame two), the pressure measured reaches up to 225 Pa. This measured pressure is larger than the sum of the expected hydrostatic pressure and capillary pressure ( $225 > 205.6$ ), therefore the capillary pressure is likely measured as well. This simplified experiment suggests the sensor likely measures the capillary pressure, however, this experiment measured the capillary pressure from an object after its shape had changed due to the flow caused by the pressure difference. For the final system, a large resistor and the rate of change of pressure will be required to measure the initial capillary pressure as explained in 4.1.

When performing the same experiment on a more complete setup to the system, which includes the substrate and a capillary tube connected to the pressure sensor, the results are very different. Instead of applying the water drop directly to the sensor, the drop is applied on the substrate, at the entrance leading to the sensor. The substrate is connected to the sensor with a capillary tube of  $ID = 250 \mu\text{m}$ , with the capillary tube being in contact with the sensor and the substrate as shown in figure 8 in section 4.2.4. The setup can be seen in Figure 16 and the results can be seen in Figure 17.

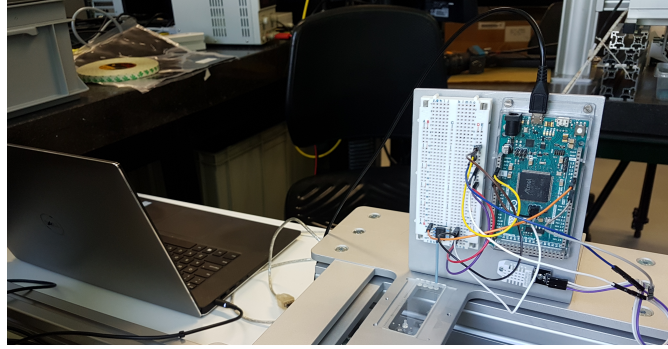


Figure 16: Experimental setup used to measure the capillary force in a droplet with the use of the substrate and capillary tube.

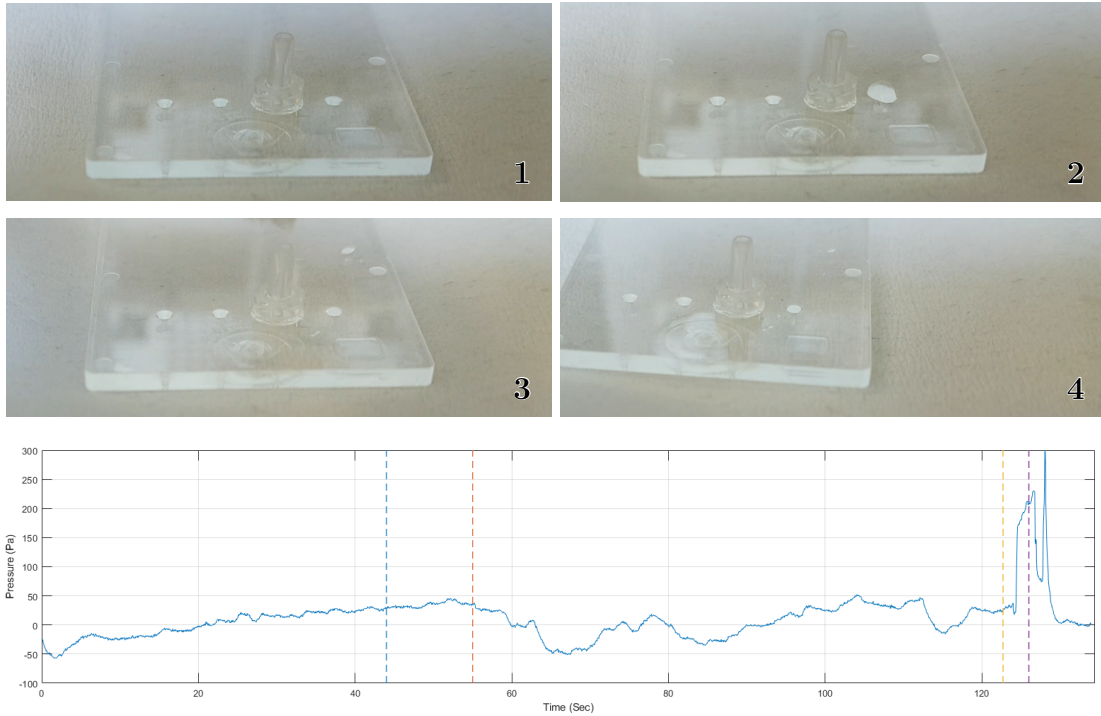


Figure 17: The data obtained when testing the capillary pressure measurement of a Sessile drop on the substrate. Each of the four frames taken from the video is placed in the timeline to determine the pressure measured by the sensor. The first frame is taken at the blue timestamp, the second frame at the red timestamp, the third frame at the yellow timestamp and the fourth frame at the purple timestamp. The second frame is right after the placement of the drop and the fourth frame shows the substrate after it has been moved.

$$P_c = \gamma * \left( \frac{2}{R} \right) = 151 \text{ Pa} \quad (27)$$

Unlike the drop on the sensor version, there is no clear increase due to the applied capillary pressure, which should be about 151 Pa. Even the baseline measurement which should remain around 0 Pa fluctuates as time passes. The largest change in pressure is due to moving the substrate as seen in frame 4. The lack of coherent pressure measurement is due to the numerous issues that can arise from a complex system. Different versions of these experiments were performed, when the drop was applied on a short capillary tube connect to pressure sensor, the capillary pressure was measured accurately. When air bubbles were present, the pressure measured was less coherent. When dead volume was introduced between the capillary tube and the sensor, the baseline would not remain around 0 Pa. There are several issues that can cause the incoherent pressure measurement, which all need to be reviewed and tested; which includes but is not limited to the following:

- Too much tension on the tubes or substrate, which can cause bending of the channel and influence the flow of liquid. In previous attempts, touching or moving the tube and substrate affected the measured pressure.
- Air bubbles or air columns may still be present in the system. Air bubbles or air columns can be created through leaks, water evaporation or absorption by the substrate. There were no visual leaks present and water absorption in the substrate is a less likely cause due to the substrate being made out of Topas, which has a water absorption of less than 0.01 % per 24 h [41]. The water absorption in the capillary tube is likelier than that of the substrate as PEEK has a water absorption of 0.10 % per 24 h, however this water absorption value is also low, in which case water absorption remains an unlikely cause [38]. Water evaporation at the entrance of the channel is a likely cause.

## 6 Conclusion and recommendations

The aim of this thesis is to develop a system to measure the capillary force for wet adhesion while not harming the frog. The design procedure of defining requirements, creating concepts and selecting the most favourable concept in terms of the requirements has been used to create a system which measures the contact area, the parameters of the meniscus and the capillary pressure with the help of a side view camera, a bottom view camera and a fixed pressure sensor. The technique of using a hydraulic resistor connected to the fixed pressure sensor used as a hydraulic capacitor was established to calculate the applied capillary pressure from the measured pressure change without the need to have the subject immobilized.

The different components necessary for the functionality of the system have been selected following the requirements set during the concept phase and by the established measurement technique. The hydraulic capacitor is selected to measure up to 10 kPa. A substrate is used as a transparent surface to apply the liquid bridge and as an entrance to the channel leading to the hydraulic capacitor. The substrate, along with a capillary tube, are selected to function as a hydraulic resistor without a hydraulic capacitance. Water is selected as an initial choice for the liquid medium in order to fill the channel and the hydraulic capacitor. The model for the system has been designed using CAD to establish how to assemble the various components. The cameras are placed in clear view of the entrance of the channel leading to the hydraulic capacitor in order to measure the contact area and meniscus parameters. The hydraulic capacitor is placed in a way to reduce tension on the capillary tube and substrate. The model includes a thermometer to monitor the temperature change as the temperature affects the system, and a force sensor to verify the functionality of the system.

After acquiring the different components to construct the system, several experiments were performed to verify the functionality of the components and to support the concept of the system. For instance, the hydraulic capacitor has been calibrated and is linear up to 10 kPa. During the hydraulic capacitance verification experiment, the hydraulic capacitance of the system was measured to be three orders of magnitude larger than the estimated hydraulic capacitance from the dimensions of the membrane of the hydraulic capacitor. Furthermore, during the support for the concept experiments, when applying a source of capillary pressure to the system, in other words when using the substrate and the capillary tube, no meaningful pressure change was measured. When applying a source of capillary pressure directly on the hydraulic capacitor, a pressure change larger than the expected value was measured, suggesting a hydraulic disconnection between the source of the capillary pressure and the hydraulic capacitor in the system. The following recommendations are given to re-evaluate the hydraulic capacitance of the system and to solve the hydraulic disconnection occurring between the capillary pressure source and the hydraulic capacitance in the system:

- The larger hydraulic capacitance is likely caused by an unknown additional source of hydraulic capacitance in the system, the source is usually in the form of air bubbles [31; 32]. To my knowledge, there are no methods that can be performed before the measurements to verify if indeed the system is free of air bubbles. There are devices that can measure flowing air bubbles in tubes but not in closed objects like the hydraulic capacitor [45]. There are measures to prevent or correct air bubble inclusion such as: absence of acute angles in fluidic path, absence of leaks, degassing liquid prior to experiments and using pressure to dissolve the air in the liquid [46]. For each of the previous experiments, the liquid was degassed prior to performing the experiment and there were no presence of leaks. It seems most promising to apply pressure up to 30 kPa, which is within the working pressure of

the sensor, before performing experiments to dissolve any potential air bubble in the liquid located in the hydraulic circuit [28]. These recommendations may also apply to solve the hydraulic disconnection between the hydraulic capacitor and the source of the capillary pressure when using the substrate and capillary tube.

- The substrate and the capillary tube may still be a source of unaccounted hydraulic capacitance in the system, however, the material of these components were considered rigid (Topas and PEEK have a Young's Modulus of 2.60 GPa and 3.95 GPa respectively) [41; 47]. If no components with higher rigidity are available, components with smaller internal volume or larger thickness may work as well [48]. The experiment performed to verify the total hydraulic capacitance can be performed again with components of different material and dimension combinations to see what works best.
- The current sampling rate is low (25 Hz) and served as a source of inaccuracy during the measurements for the evaluation of the hydraulic capacitance. The measurements would reach the applied pressure within 0.2 s leaving a few points (4-8 points) to apply a fitting curve. The sampling rate of the pressure data acquisition should be improved, which can be done by using a faster serial reader software such as Matlab instead of Arduino. Additionally, the pressure data acquisition can be implemented to run with the cameras and force sensor in synchronisation when using Matlab to facilitate the capillary force experiment intended to verify the functionality of the system.

When applying a capillary pressure from a simple drop directly on the hydraulic capacitor, the measured pressure was larger than the expected capillary pressure, which suggests the system can measure the capillary pressure. However, the uncertainty of the hydraulic capacitance and the lack of pressure measured, when using substrate and the capillary tube, needs to be solved before performing the intended capillary force experiment with shape analysis and a force sensor to verify the full functionality of the system. More knowledge on microfluidics and hydraulic circuits could prove beneficial in this endeavor, specifically knowledge on how liquid pressure and liquid flow behave in microchannels and how they can be measured.

## References

- [1] A. Jagota and C.-Y. Hui, “Adhesion, friction, and compliance of bio-mimetic and bio-inspired structured interfaces,” *Materials Science and Engineering: R: Reports*, vol. 72, no. 12, pp. 253–292, Dec. 2011. [Online]. Available: <http://www.sciencedirect.com/science/article/pii/S0927796X1100060X> (Accessed 2020-09-03).
- [2] J. Eisenhaure and S. Kim, “A Review of the State of Dry Adhesives: Biomimetic Structures and the Alternative Designs They Inspire,” *Micromachines; Basel*, vol. 8, no. 4, p. 125, 2017, num Pages: 125 Place: Basel, Switzerland, Basel Publisher: MDPI AG. [Online]. Available: <https://search.proquest.com/docview/1899818069/abstract/5AA42C1904664512PQ/1> (Accessed 2020-09-03).
- [3] A. P. Russell, A. Y. Stark, and T. E. Higham, “The Integrative Biology of Gecko Adhesion: Historical Review, Current Understanding, and Grand Challenges,” *Integrative and Comparative Biology*, vol. 59, no. 1, pp. 101–116, Jul. 2019, publisher: Oxford Academic. [Online]. Available: <https://academic.oup.com/icb/article/59/1/101/5486592> (Accessed 2020-09-03).
- [4] J. K. A. Langowski, D. Dodou, M. Kamperman, and J. L. van Leeuwen, “Tree frog attachment: mechanisms, challenges, and perspectives,” *Frontiers in Zoology*, vol. 15, no. 1, p. 32, Aug. 2018. [Online]. Available: <https://doi.org/10.1186/s12983-018-0273-x> (Accessed 2020-03-03).
- [5] J. K. Schöning-Langowski, “Getting a grip on tree frog attachment : structures, mechanisms, and biomimetic potential,” Ph.D. dissertation, Wageningen University, Wageningen, 2019, iSBN: 9789463431859. [Online]. Available: <https://edepot.wur.nl/471878>
- [6] A. Moghadam and H. Vahedi Tafreshi, “On liquid bridge adhesion to fibrous surfaces under normal and shear forces,” *Colloids and Surfaces A: Physicochemical and Engineering Aspects*, vol. 589, p. 124473, Feb. 2020. [Online]. Available: <https://linkinghub.elsevier.com/retrieve/pii/S0927775720300650> (Accessed 2020-03-18).
- [7] V. Liimatainen, M. Vuckovac, V. Jokinen, V. Sariola, M. J. Hokkanen, Q. Zhou, and R. H. A. Ras, “Mapping microscale wetting variations on biological and synthetic water-repellent surfaces,” *Nature Communications*, vol. 8, no. 1, pp. 1–7, Nov. 2017, number: 1 Publisher: Nature Publishing Group. [Online]. Available: <https://www.nature.com/articles/s41467-017-01510-7> (Accessed 2020-03-11).
- [8] J. C. de Graaff, D. Th. Ubbink, S. M. Lagarde, and M. J. Jacobs, “The Feasibility and Reliability of Capillary Blood Pressure Measurements in the Fingernail Fold,” *Microvascular Research*, vol. 63, no. 3, pp. 270–278, May 2002. [Online]. Available: <https://linkinghub.elsevier.com/retrieve/pii/S002628620192388X> (Accessed 2020-04-14).
- [9] N. Nagy, “Contact Angle Determination on Hydrophilic and Superhydrophilic Surfaces by Using  $r$ - $\theta$ -Type Capillary Bridges,” *Langmuir*, vol. 35, no. 15, pp. 5202–5212, Apr. 2019, publisher: American Chemical Society. [Online]. Available: <https://doi.org/10.1021/acs.langmuir.9b00442> (Accessed 2020-03-13).
- [10] E. Portuguese, A. Alzina, P. Michaud, M. Oudjedi, and A. Smith, “Evolution of a Water Pendant Droplet: Effect of Temperature and Relative Humidity,” *Natural Science*, vol. 09, pp. 1–20, Jan. 2017.

- [11] Y. Liu, M. Mutailipu, L. Jiang, J. Zhao, Y. Song, and L. Chen, "Interfacial tension and contact angle measurements for the evaluation of CO<sub>2</sub>-brine two-phase flow characteristics in porous media," *Environmental Progress & Sustainable Energy*, vol. 34, no. 6, pp. 1756–1762, 2015, eprint: <https://onlinelibrary.wiley.com/doi/pdf/10.1002/ep.12160>. [Online]. Available: <http://aiche.onlinelibrary.wiley.com/doi/abs/10.1002/ep.12160> (Accessed 2020-03-18).
- [12] "Surface Tension," Oct. 2013, library Catalog: [chem.libretexts.org](http://chem.libretexts.org). [Online]. Available: [https://chem.libretexts.org/Bookshelves/Physical\\_and\\_Theoretical\\_Chemistry\\_Textbook\\_Maps/Supplemental\\_Modules\\_\(Physical\\_and\\_Theoretical\\_Chemistry\)/Physical\\_Properties\\_of\\_Matter/States\\_of\\_Matter/Properties\\_of\\_Liquids/Surface\\_Tension](https://chem.libretexts.org/Bookshelves/Physical_and_Theoretical_Chemistry_Textbook_Maps/Supplemental_Modules_(Physical_and_Theoretical_Chemistry)/Physical_Properties_of_Matter/States_of_Matter/Properties_of_Liquids/Surface_Tension) (Accessed 2020-07-07).
- [13] H.-J. Butt and M. Kappl, "Normal capillary forces," *Advances in Colloid and Interface Science*, vol. 146, no. 1, pp. 48–60, Feb. 2009. [Online]. Available: <http://www.sciencedirect.com/science/article/pii/S0001868608001899> (Accessed 2020-03-18).
- [14] S. Kwon, B. Kim, S. An, W. Lee, H.-Y. Kwak, and W. Jhe, "Adhesive force measurement of steady-state water nano-meniscus: Effective surface tension at nanoscale," *Scientific Reports*, vol. 8, no. 1, pp. 1–7, May 2018, number: 1 Publisher: Nature Publishing Group. [Online]. Available: <https://www.nature.com/articles/s41598-018-26893-5> (Accessed 2020-04-06).
- [15] T. Endlein and W. Barnes, "Wet Adhesion in Tree and Torrent Frogs," Jan. 2016, pp. 4355–4373.
- [16] H. Lillywhite, "Thermal modulation of cutaneous mucus discharge as a determinant of evaporative water loss in the frog, *Rana catesbeiana*," *Zeitschrift für Vergleichende Physiologie*, vol. 73, no. 1, pp. 84–104, 1971.
- [17] E. H. Larsen and H. Ramløv, "Role of cutaneous surface fluid in frog osmoregulation," *Comparative Biochemistry and Physiology Part A: Molecular & Integrative Physiology*, vol. 165, no. 3, pp. 365–370, Jul. 2013. [Online]. Available: <https://www.sciencedirect.com/science/article/pii/S1095643313001001> (Accessed 2021-10-05).
- [18] D.-M. Drotlef, L. Stepien, M. Kappl, W. J. P. Barnes, H.-J. Butt, and A. d. Campo, "Insights into the Adhesive Mechanisms of Tree Frogs using Artificial Mimics," *Advanced Functional Materials*, vol. 23, no. 9, pp. 1137–1146, 2013, eprint: <https://onlinelibrary.wiley.com/doi/pdf/10.1002/adfm.201202024>. [Online]. Available: <https://onlinelibrary.wiley.com/doi/abs/10.1002/adfm.201202024> (Accessed 2020-04-14).
- [19] W. J. P. Barnes, M. Baum, H. Peisker, and S. N. Gorb, "Comparative Cryo-SEM and AFM studies of hylid and rhacophorid tree frog toe pads," *Journal of Morphology*, vol. 274, no. 12, pp. 1384–1396, 2013, eprint: <https://onlinelibrary.wiley.com/doi/pdf/10.1002/jmor.20186>. [Online]. Available: <http://onlinelibrary.wiley.com/doi/abs/10.1002/jmor.20186> (Accessed 2021-10-05).
- [20] "i-SPEED 7 high speed slow mo camera." [Online]. Available: <https://www.ix-cameras.com/7-Series/> (Accessed 2021-06-01).

- [21] M. Andrews, “Best Slow Motion Camera – Top 7 Picks (NEW Guide),” Aug. 2020. [Online]. Available: <https://camerasgear.com/best-slow-motion-camera/> (Accessed 2021-06-01).
- [22] “Why are Thermal Imaging Cameras So Expensive? An Ultimate Guide to IR!” [Online]. Available: <https://novatestpro.com/pages/why-are-thermal-imaging-cameras-so-expensive> (Accessed 2021-06-01).
- [23] “Handheld Thermal Cameras | FLIR Industrial | Teledyne FLIR.” [Online]. Available: <https://www.flir.com/browse/industrial/handheld-thermal-cameras/> (Accessed 2021-06-01).
- [24] “Infrared Cameras.” [Online]. Available: <https://www.infratec.eu/thermography/infrared-camera/> (Accessed 2021-06-01).
- [25] JAI, “Area Scan Cameras,” Mar. 2021, archive Location: [//www.jai.com/](http://www.jai.com/) Publisher: JAI. [Online]. Available: [//www.jai.com/products/area-scan-cameras](http://www.jai.com/products/area-scan-cameras) (Accessed 2021-06-01).
- [26] “Area scan camera.” [Online]. Available: <https://www.stemmer-imaging.com/en-nl/products/category/area-scan-cameras/> (Accessed 2021-06-01).
- [27] “Pressure Mapping Sensors,” Dec. 2014. [Online]. Available: <https://www.tekscan.com/pressure-mapping-sensors> (Accessed 2021-06-01).
- [28] “TruStability™ SSC Pressure Sensors | Honeywell.” [Online]. Available: <https://sps.honeywell.com/us/en/products/sensing-and-iot/sensors/pressure-sensors/board-mount-pressure-sensors/trustability-ssc-series> (Accessed 2021-05-19).
- [29] “Precise and Effective Force Sensors & Load Cells | Althen Sensors.” [Online]. Available: <https://www.althensensors.com/sensors/force-sensors/> (Accessed 2021-06-01).
- [30] “Force Measurement Sensor | How it Works | FUTEK.” [Online]. Available: <https://www.futek.com/force-measurement> (Accessed 2021-06-01).
- [31] B. J. Kirby, “Micro- and Nanoscale Fluid Mechanics: Transport in Microfluidic Devices,” p. 536, Oct. 2010.
- [32] P. Sharma, “Coupled electrokinetic fluxes in a single nanochannel for energy conversion,” phdthesis, Université Grenoble Alpes, Apr. 2017. [Online]. Available: <https://tel.archives-ouvertes.fr/tel-02000980> (Accessed 2021-05-19).
- [33] “Arduino - Products.” [Online]. Available: <https://www.arduino.cc/en/Main/Products> (Accessed 2020-09-10).
- [34] “Properties: A Background to Silicon and its Applications.” [Online]. Available: <https://www.azom.com/properties.aspx?ArticleID=599> (Accessed 2021-06-02).
- [35] “Capillary action,” May 2021, page Version ID: 1025831919. [Online]. Available: [https://en.wikipedia.org/w/index.php?title=Capillary\\_action&oldid=1025831919](https://en.wikipedia.org/w/index.php?title=Capillary_action&oldid=1025831919) (Accessed 2021-06-04).
- [36] W. K. Schomburg, *Introduction to Microsystem Design*, ser. RWTHedition. Berlin Heidelberg: Springer-Verlag, 2011. [Online]. Available: <https://www.springer.com/gp/book/9783642268526> (Accessed 2021-05-19).

- [37] “Straight Channel Chips with Four Parallel Channels - Fluidic 143.” [Online]. Available: <https://www.microfluidic-chipshop.com/catalogue/microfluidic-chips/polymer-chips/straight-channel-chips-microscopy-slide-format/straight-channel-chips-with-four-parallel-channels-fluidic-143/> (Accessed 2021-05-19).
- [38] “PEEK (Polyetheretherketone) | Poly-Tech Industrial.” [Online]. Available: <https://www.polytechindustrial.com/products/plastic-stock-shapes/peek> (Accessed 2021-06-25).
- [39] “Durometer Shore Hardness Scale.” [Online]. Available: <https://www.smooth-on.com/page/durometer-shore-hardness-scale/> (Accessed 2021-06-25).
- [40] “PEEK Tubing Natural 360µm OD x25µm ID x5ft.” [Online]. Available: <https://www.idex-hs.com/store/fluidics/fluidic-connections/tubing/high-pressure-tubing/peek-tubing/peek-tubing-natural-360-m-od-x25-m-id-x5ft.html> (Accessed 2021-05-19).
- [41] “Advanced COC Polymers | TOPAS.” [Online]. Available: <https://topas.com/> (Accessed 2021-06-21).
- [42] “DHT 22 - Joy-IT.” [Online]. Available: <https://joy-it.net/en/products/SEN-DHT22> (Accessed 2021-05-19).
- [43] “Load Cells | Load Cells - for online sales of Sensors & Transducers| RS Components.” [Online]. Available: <https://nl.rs-online.com/web/c/automation-control-gear/sensors-transducers/load-cells/?searchTerm=force%20sensor> (Accessed 2020-09-10).
- [44] “Thorlabs - PT3-Z8 25 mm (0.98”) Three-Axis Motorized Translation Stage, 1/4”-20 Taps.” [Online]. Available: <https://www.thorlabs.com/thorproduct.cfm?partnumber=PT3-Z8> (Accessed 2021-05-19).
- [45] “Sensors for Non-invasive Air Bubble Detection – SONOCHECK · SONOTEC.” [Online]. Available: <https://www.sonotec.eu/en/products/non-invasive-fluid-monitoring/air-bubble-detection/> (Accessed 2021-10-28).
- [46] T. E. Team, “Air bubbles and microfluidics,” *Elveflow*, Feb. 2021, publisher: Elveflow. [Online]. Available: <https://www.elveflow.com/microfluidic-reviews/general-microfluidics/air-bubbles-and-microfluidics/> (Accessed 2021-10-28).
- [47] “Properties: Supplier Data - Polyetheretherketone ( PEEK ) ( Goodfellow ).” [Online]. Available: <https://www.azom.com/properties.aspx?ArticleID=1882> (Accessed 2021-10-21).
- [48] “Microfluidics/Hydraulic resistance and capacity - Wikibooks, open books for an open world.” [Online]. Available: [https://en.wikibooks.org/wiki/Microfluidics/Hydraulic\\_resistance\\_and\\_capacity](https://en.wikibooks.org/wiki/Microfluidics/Hydraulic_resistance_and_capacity) (Accessed 2021-10-14).

## Appendix

### A Calculations to support the component selection

Figure 18 shows the theoretical time constants obtained from the calculated hydraulic capacitance of the pressure sensor and the resistance determined from different options of substrate and tubing combinations. These results were obtained following the liquid properties of water, as the viscosity of the liquid medium affects the time constant. The desired time constant should reach approximately 5 s, enough to determine the rate of change in pressure over time. The combination of the fluidic 143 substrate and PEEK 25 tube give the best result which can be further improved by increasing the length of the PEEK 25 tube.

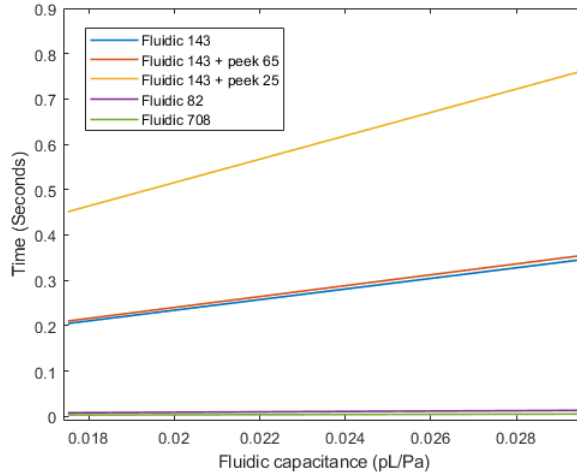


Figure 18: Comparing the time constant of the system using different substrate/tube combinations. The fluidics are the substrate with each a different channel width and length. The 143 has a width of 20  $\mu\text{m}$  and length of 58.5 mm; the 82 has a width of 50  $\mu\text{m}$  and length of 87 mm; and the 708 has a width of 200  $\mu\text{m}$ , a height of 100  $\mu\text{m}$  and a length of 1879 mm. The PEEK are the capillary tubes with an inner diameter of 65  $\mu\text{m}$  or 25  $\mu\text{m}$  and with a length of 135 mm.

### B Additional support to neglect the hydraulic capacitance of the substrate

The hydraulic capacitance of a channel can be roughly estimated from equation 28 [48].  $K$  is the dilatibility which can be approximated as the inverse of the Young modulus of the material and  $V$  is the volume of the channel. The hydraulic capacitance of the substrate can be roughly estimated to be around  $7.8 * 10^{-21} \text{ m}^3 \text{ Pa}^{-1}$  which is around 4 orders of magnitude lower than the expected hydraulic capacitance of the sensor. This suggests the hydraulic capacitance of the channel is insignificant to the hydraulic capacitance of the whole system and thus can be neglected.

$$C = K * V \quad (28)$$

The membrane is made out of silicon, which has a larger Young's modulus than Topas (110 GPa > 2.60 GPa) but the membrane remains deformable thanks to its thickness [34; 41]. The thinnest wall of the substrate is  $7.4 * 10^{-4}$  m thick which is 81 times larger than that of the membrane. This difference in size supports the reasoning that the membrane has a much larger hydraulic capacitance than the substrate even if the materials share similar hardness.

## C Future steps to accomplish

- Finish evaluating the hydraulic capacitance of the sensor and solve the issue of the lack of pressure measurement when the sensor is connected to the substrate.
- Modify the Arduino script to increase sampling frequency.
- Create a matlab script to read the sensor data with known sampling frequency and official start time.
- Create a matlab script to run the sensor, the camera and the force sensor in synchronisation.
- With the higher sampling frequency, do a frequency analysis of potential vibrations of the system.
- Modify the system to include any necessary vibration dampening components.
- Test the system with a three-way comparison: capillary pressure measured by the sensor, image analysis and force sensor.
- If the system succeeds at measuring the capillary force, modify the substrate to accommodate tree frogs and modify the system to be able to change the orientation of the substrate.

## D Verification of the hydraulic capacitance verification method

The method used to verify the hydraulic capacitance in section ?? can be proven by performing the experiment with two differently sized capillary tubes. The time constant for each of the capillary tubes can be determined through the experiment; the time constant of the larger tube is used to determine a hydraulic capacitance using equation 29. The hydraulic capacitance should not change in between experiments as long as air bubbles are not introduced in the system. The calculated hydraulic capacitance can be used in conjunction with the time constant of the smaller tube to calculate the ID of the smaller tube by using equation 30. If the experiment method is valid, the calculated ID of the smaller tube should match the advertised and measured ID. In this case, using a 500  $\mu\text{m}$  ID to determine the capacitance results in a calculated ID of the smaller tube of 287  $\mu\text{m}$ , which is within an error of 12%, see table 4. Using longer capillary tubes can help increase the precision of the experiment if necessary, here both tubes were about 53 mm long. This shows the method works and the issues are related to the total hydraulic capacitance of the experiment.

$$C = \frac{\tau_{large} * \pi * R_{large}^4}{8 * \nu * L_{large}} \quad (29)$$

$$R_{small} = \sqrt[4]{\frac{8 * \nu * L_{small} * C}{\pi * \tau_{small}}} = 287 \mu\text{m} \quad (30)$$

	Inner Diameter ( $\mu\text{m}$ )
Calculated	287
Advertised	254
Measured	248, see figure 19

Table 4: The inner diameter of the capillary tube determined in different ways.

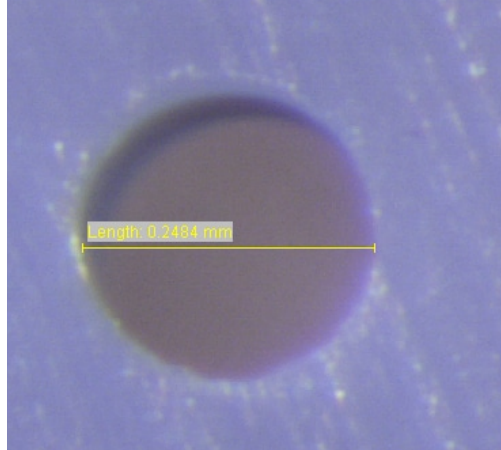


Figure 19: The inner diameter of the capillary tube determined through a microscope.

## E Air bubble effect on hydraulic capacitance

According to figure 20, the lower the hydraulic capacitance of a pressure sensor, the larger the effect an air bubble will have on the total capacitance of the system. In this case, the initial capacitance is in the range of 0.01 pL/Pa to 0.03 pL/Pa which means even an air to fluid volume ratio of  $10^{-4}$  or lower will greatly increase the total capacitance.

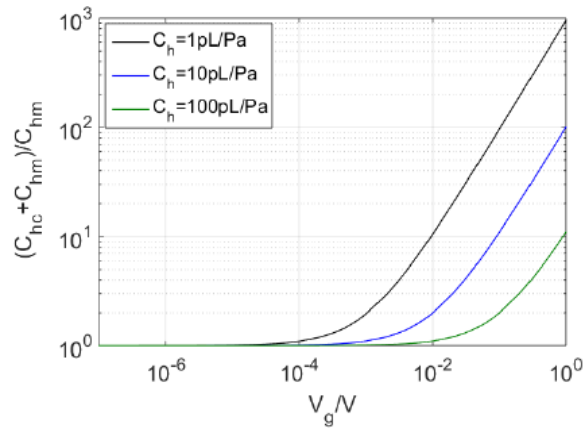


Figure 20: Effect of the presence of gas bubbles on the capacitance depending on the initial capacitance of the sensor [32].

## F Vibrations additional details

Across the different experiments performed during this thesis, it is clear that vibrations effect the system, either through the fluidic medium or through the physical medium around the sensor. During the time constant experiments, vibrations are measured by the sensor when opening and closing the different valves, possibly due to certain dead volume present in these valves. The vibrations were lessened by applying a damper on the valves, which was done by attaching the valves to a heavy object as seen in figure 21. The difference in vibrations can be seen in figure 22.

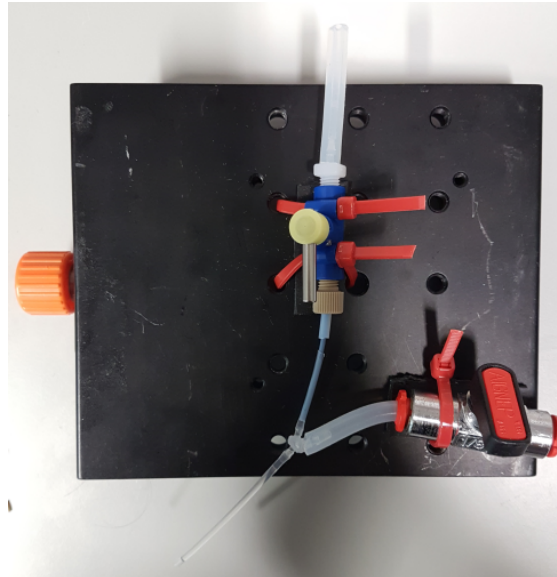


Figure 21: Damper system added to the valves to reduce vibrations.

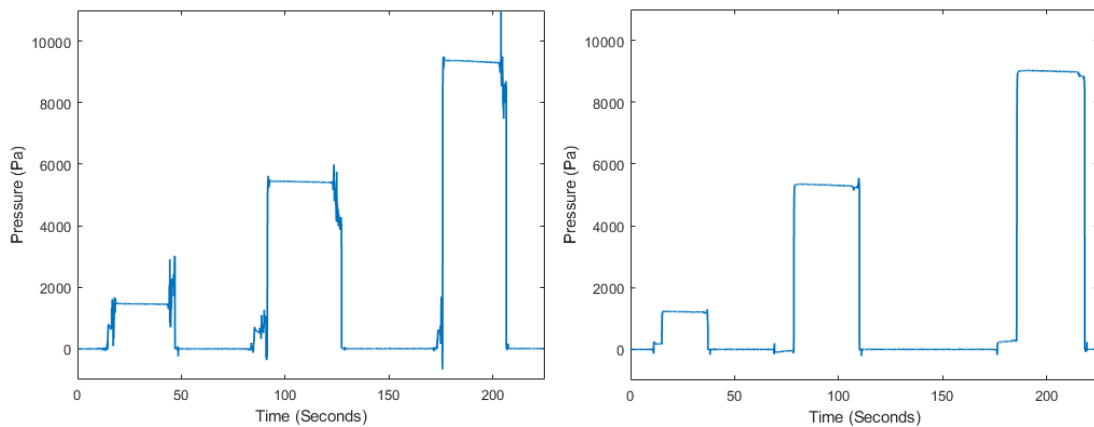


Figure 22: Data obtained without the damper system (left) and with the damper system (right).

Vibrations can also be seen directly on the system when moving the bracket the sensor is located on. This may be due to the movement of the tube relative to the system and may be reduced by taking harder tubes. This supports the potential issue of measuring vibrations through the bracket if the bracket is made too tall without enough support.

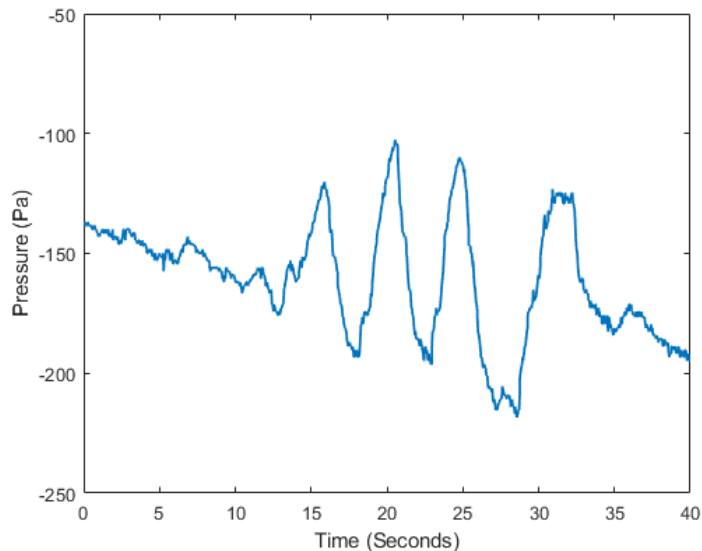


Figure 23: Pressure measured when moving the bracket the sensor is located on.

## G Proof of concept experiments additional details

Pixel measurements were performed in order to calculate the expected pressure during the additional support for the concept in section 5.4. The size of the bubble is measured in pixels, see figure 24, which is converted to metrics using an in picture reference of known size as seen in equation 31. The reference used is the dimension of the pressure sensor. The reference is 22 pixels long in the picture with a true length of 1.93 mm long [28]. The diameter of the liquid drop is 17 pixels long which means the drop has a true diameter of 1.5 mm. The height of the liquid drop is 12 pixels long which means the drop has a true height of 1.1 mm.

$$Object_{true} = \frac{Object_{pixel} * Reference_{true}}{Reference_{pixel}} \quad (31)$$

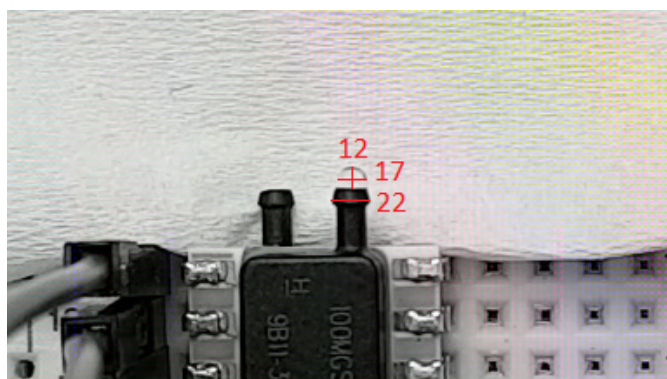


Figure 24: Pixel measurement of the liquid drop applied on the sensor

During the single drop on the pressure sensor to prove the working principle of the system in section 5.4, different variations were performed. The variations include connecting a capillary tube to the sensor, figure 25, presence of air bubbles in between the capillary tube and the sensor, figure 26, and dead volume present in between the capillary tube and the sensor figure 27. The capillary force is still being measured when a capillary tube is used, although the maximum value is reached slower due to the increased time constant from the higher resistance of the tube. When air bubbles are included, the systems reaction is much slower and when dead volume is included, the system does not remain stable.

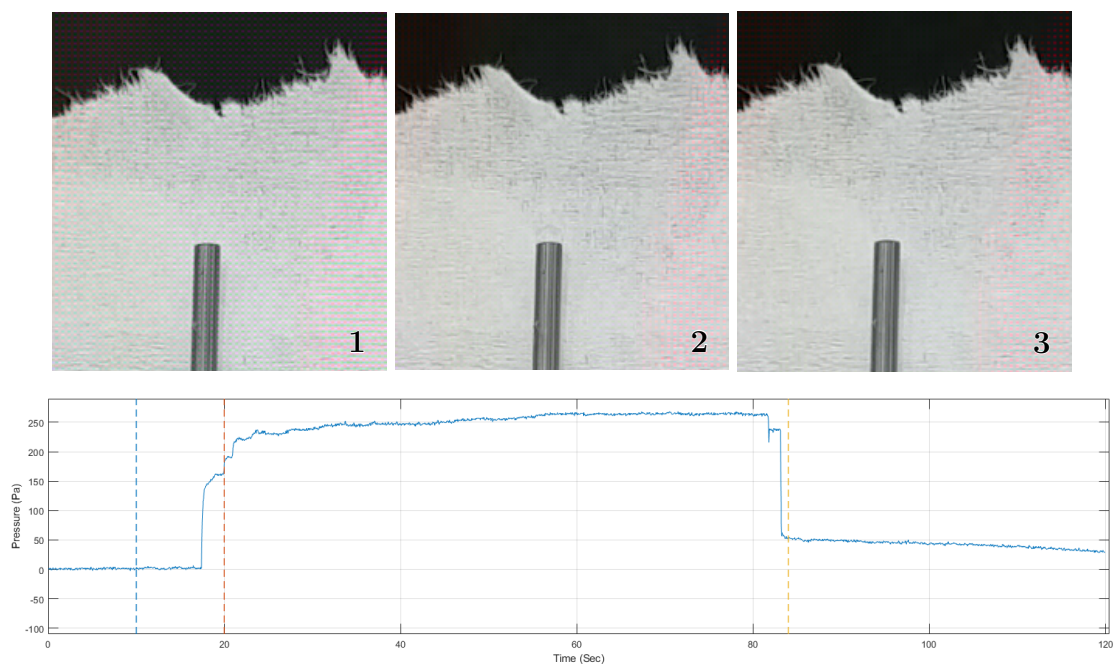


Figure 25: The data obtained when testing the capillary pressure measurement of a Sessile drop on the capillary. Each of the three frames taken from the video is placed in the timeline to determine the pressure measured by the sensor. The first frame is taken at the blue timestamp, the second frame at the red timestamp and the third frame at the yellow timestamp.

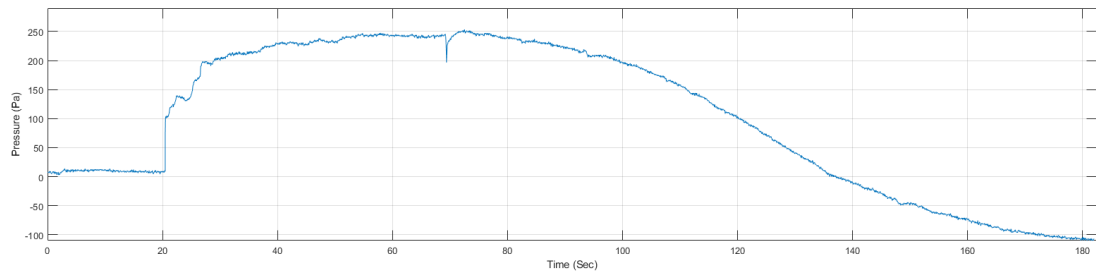


Figure 26: The data (bottom) obtained when testing the capillary pressure measurement of a Sessile drop on the capillary which included air bubbles (top).

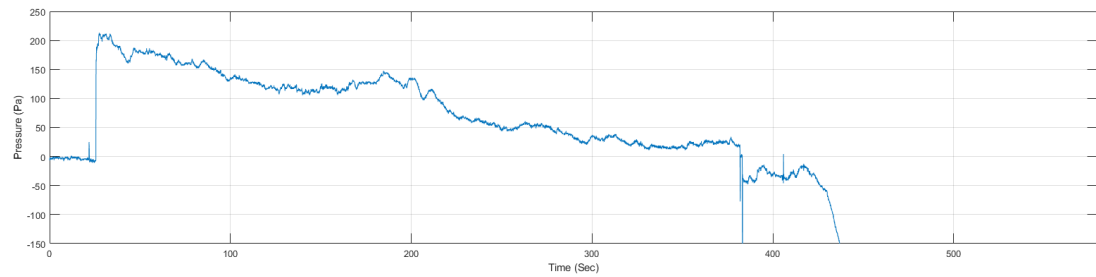
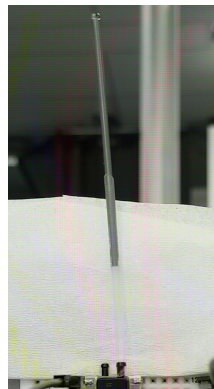


Figure 27: The data (bottom) obtained when testing the capillary pressure measurement of a Sessile drop on the capillary which included significant dead volume (top).